Preparation and Characterisation of Hierarchical Zeolite Catalysts

Zélia Joana Lopes

Thesis to obtain the Master of Science Degree in

Chemical Engineering

Supervisors: Prof. Dr Carlos Manuel Faria de Barros Henriques

Dr Vladimir L. Zholobenko

Examination Committee

Chairperson:	Prof. Dr Francisco Manuel da Silva Lemos
Supervisor:	Prof. Dr Carlos Manuel Faria de Barros Henriques
Member of the Committee:	Prof. Dr José Manuel Félix Madeira Lopes

November 2017

Acknowledgments

I would first like to express my biggest gratitude to Dr Vladimir Zholobenko for all his support, dedication and availability for anything I needed. I would also like to express my gratitude to Prof. Carlos Henriques for all his help and guidance throughout this work.

I would like to thank everyone at the Birchall Centre for their kindness, and for always making me feel welcome. To Aqeel, for all his help with my work and with my adaptation; without him my work would not be possible, as he designed and optimised most of the procedures used. A special thank you to Cátia who made everything easier and more like home. Having someone from my own country, speaking my mother tongue, always available to help, talk or go out has made my stay at Keele much better.

I also want to thank all my friends from Portugal, Carolina, Leonor, Ricardo, Rita, “E Jeropiga” and “Equipa” for being present even at a distance and helping me through the toughest times. A very very special thank you to Marta, who was my rock and gave me strength every day. Thank you for believing in me since day one and for never letting me think I was alone.

Last but not least, I would like to thank my parents for all their support, for the Skype chats that made me feel at home, for all their love and patience and for providing me with this opportunity.

Abstract

Biodiesel is one of the most important fuels, given its high combustion efficiency (it has a strong tendency to auto-ignite). The blendstock for this type of fuels are middle distillates obtained from hydrocracking, thus the need to improve the efficiency of hydrocracking catalysts in terms of selectivity.

Zeolite Y is the most widely used catalyst for these processes, due to its high thermal stability, density of acid sites and rather high acid strength. However, it also produces a large amount of light distillates. Hence, modifying zeolite Y to increase the mesoporosity can improve the yield of middle distillates: with bigger pores, more middle distillates can be obtained.

The main goal of this work was to create hierarchical mesoporosity in zeolite Y. The starting material was zeolite Y in the NaY form, and two different routes were experimented: the zeolite was ion exchanged to NH4Y form and then underwent an acid treatment to create mesopores (Route 1); the zeolite suffered the acid treatment and was ion exchanged subsequently (Route 2). In the end of both routes, a calcination step took place to remove the formed NH_3.

The following characterisation techniques were used: N_2 sorption, XRD, FTIR and SEM/EDS. In FTIR, two experiences were made: pyridine was used to characterise the acid sites in zeolite Y (number and type) and different probe molecules were used to test pore accessibility.

Results showed that Route 2 is preferable, since the loss of crystallinity was smaller and the amount of acid sites was higher.

Keywords: zeolite, FAU, characterization, modification, preparation, mesoporous, catalyst, biodiesel

Resumo

O biodiesel é um dos combustíveis mais importantes, devido à sua alta eficiência de combustão (tem uma elevada tendência para autoignição). É produzido a partir de destilados médios obtidos através do *hydrocraking*, daí a necessidade de melhorar a eficiência dos catalisadores de *hydrocraking* em termos de seletividade.

O zeólito Y é o catalisador mais usado nestes processos, graças à sua estabilidade térmica, densidade de centros ácidos e elevada força ácida. Contudo, também produz alguns destilados leves. Consequentemente, modificar o zeólito Y para aumentar a mesoporosidade pode melhorar o rendimento em destilados médios.

O objetivo deste trabalho foi criar mesoporosidade hierárquica no zeólito Y. O material de partida foi o zeólito Y na forma NaY, e foram ensaiadas: Via 1, em que o zeólito sofreu permuta iónica para a forma NH4Y e depois sofreu o tratamento ácido para criar mesoporos e Via 2, em que o zeólito sofreu o tratamento ácido e permuta iónica posteriormente. No final de ambas as vias houve uma calcinação para remover o NH_3.

As técnicas de caracterização usadas foram: sorção de N_2, RD, FTIR e SEM/EDS. Na técnica FTIR, foram feitas duas experiências: usou-se piridina para quantificar os centros ácidos no zeólito Y e diferentes moléculas sonda foram usadas para testar a acessibilidade dos poros.

Os resultados mostraram que a Via 2 é preferível, visto que a perda de cristalinidade foi menor e a quantidade de centros ácidos maior.

Palavras-chave: zeólito, FAU, caracterização, modificação, preparação, mesoporos, catalisador, biodiesel

Table of contents

List of figures

List of tables

Nomenclature

- a.u. – Arbitrary units
- BAS – Brønsted acid sites
- BET – Brunauer-Emmett-Teller
- CBU – Composite building unit(s)
- DFT – Density functional theory
- EDS – Energy-dispersive X-ray spectroscopy
- EFAL – Extra-framework aluminium
- FAAE – Fatty Acid Alkyl Esters
- FAU – Faujasite
- FTIR – Fourier Transform Infrared Spectroscopy
- IE – Ion exchange
- IR – Infrared
- IUPAC – International Union of Pure and Applied Chemistry
- IZA – International Zeolite Association
- LAS – Lewis acid sites
- MAS – Magnetic-Angle Spinning
- meq – milliequivalents
- NMR – Nuclear Magnetic Resonance
- PBU – Primary building unit(s)
- Py – Pyridine
- RT – Room temperature
- SBU – Secondary building unit(s)
- SEM – Scanning electron microscopy
- XRD – X-ray diffraction

1. Introduction

Diesel fuel is an important fuel, given its high combustion efficiency: ignition is simpler, since it does not need a spark; diesel is denser than petrol which means that it releases more energy; diesel fuel has much more lubrication. In the last few years, diesel fuel has been in short supply, and its demand has been increasing significantly. Therefore, there is an urge to increase the yield of diesel fuels to meet the market's current demand. [1]

Middle distillates, obtained from hydrocracking, are treated and blended into diesel fuels. Hence the need to improve the efficiency of hydrocracking catalysts.

The most widely used catalyst for hydrocracking processes is zeolite Y [2], because of its rather high acid strength, higher hydrothermal stability, density of acid sites and large hydrogen-transfer capacity. Although it has better performance than other materials, it is not enough to satisfy the maximum yield of middle distillates, since it also produces a large amount of light distillates. Besides, zeolite Y is scarce in mesopores, there is no point in trying to enhance the conversion of large molecules because of diffusion limitations. [1]

Modifying zeolite Y to create mesopores can improve the yield of middle distillates in the hydrocracking process. However, to allow middle distillates to enter the pores, the mesopores need to be accessible from the external surface. This is the main difference from the commercial existing mesoporous zeolites, since they only have mesopores inside the framework. The process of creating mesopores is complicated because the modifying conditions have to be very strict, and even so the zeolite loses crystallinity. [1]

The effect of zeolite Y crystallite size on the hydrocracking activity has been studied, and it was concluded that the catalyst with a smaller crystallite size (bigger pore size) Y zeolite exhibits higher middle distillate selectivity. Usually, the hydrocracking activity is related to the number of acid sites. Yet, a smaller crystallite size of zeolite Y has less acid sites. What improves the hydrocracking activity is the larger amount of available acid sites due to higher surface area and creation of mesopores.

The most versatile biodiesel catalysts are zeolites due to their pore distribution and chemical composition. Basic catalysts are preferred over acid catalysts, due to its faster reaction rate and mild reaction conditions. However, in order to understand basicity of zeolites, it is necessary to study their acidity as well. The aim of this research is to generate quantitative data on the concentration and location of the acid sites, and therefore, the potential role of the acid centres in catalytic reactions, hence providing a basis for the design of new heterogeneous catalysts with high activity, selectivity and stability.

Following this introduction, comes a literature review on zeolites. Afterwards, the procedures and techniques used are described, with the subsequent results featured and discussed. To finalise, there is a chapter with the main conclusions of this work and suggestions for future work.

2. Zeolites

The first zeolite was discovered by a Swedish mineralogist, Cronsted, and he named it zeolite due to the Greek terms '*zeo*' meaning "to boil" and '*lithos*' meaning "stone". [3]

Zeolites are crystalline aluminosilicates based on an infinite extending three-dimensional, four-connected framework consisting of AlO_4 and SiO_4 tetrahedra linked to each other by sharing one oxygen atom. Each AlO_4 in the framework bears a net negative charge which is balanced by extra-framework cations of hydrogen or of alkali or alkali-earth metals, such as sodium, potassium, magnesium or calcium or even transition metal entities. [4] [5] The resulting structure (figure 1) is highly porous and contains channels and cavities of molecular dimensions that are occupied by cations and water – the zeolite's pores.

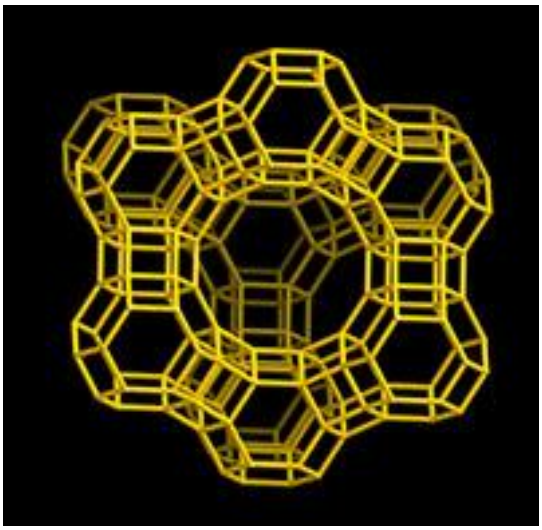

Figure 1 - Zeolite (Faujasite) structure [International Zeolite Association – IZA]

Due to its porous structure and the ability to separate mixtures of molecules (in both gas and liquid phases) on the basis of their effective sizes, zeolites are often used as molecular sieves. When the water present in the pores is removed, the voids created within the framework are able to take in other molecules. This process is called sorption. [3]

Zeolites can be natural or synthetic. Natural zeolites originate from volcanic rock that are formed by hydrothermal crystallization of reactive alkali metal aluminosilicate gels at low temperatures (<100^{o}C)

and under alkaline conditions. On the other hand, synthetic zeolites are essentially prepared by mixing a Si source and an Al source in a strongly basic aqueous solution. The main factors to determine what structure is formed are the silica-to-alumina ratio, the nature of the compensating cations, and the synthesis temperature of the resultant gel. Currently there are over 200 synthetic zeolites and 67 natural occurring zeolites. [5] [6] [7]

2.1. Structure

All zeolites have framework structures consisting of TO_4 tetrahedra, where T represents a Si atom or a Al atom connected by an oxygen atom. They are assembled in a way that the oxygen at each corner is shared with identical Si or Al tetrahedra. [3]

Each TO_4 unit is called a Primary Building Unit (PBU). The linkage between two PCU originates a Secondary Building Unit (SBU) that connects to other SBU for a determined number of times generating the Composing Building Units (CBU). Based on the possible variations in the framework of zeolites, a “structure code” has been assigned to each one of them, for the sake of simplicity in their identification. These structure codes have been proposed by the Structure Commission of the International Zeolite Association (IZA-SC) and consists of a three-letter code derived from the name of the zeolite or “type material”, e.g. FAU is for Faujasite. A detailed compilation of framework types can be found in the *Atlas of Zeolite Framework Types*. [7] [8]

Besides the structure type, zeolites can also be classified by the number of oxygen atoms in the pore openings (figure 2).

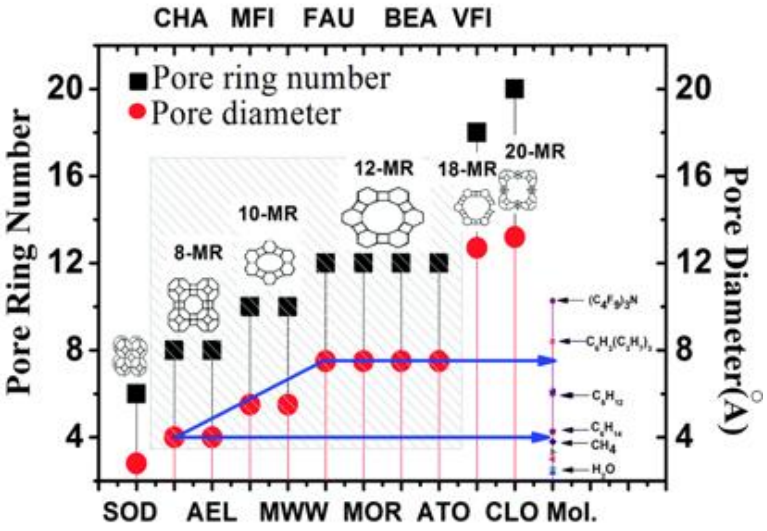

Figure 2 - Relationship between molecular diameter, pore diameter and pore ring [9]

By definition, zeolites are microporous materials. A material can be defined as microporous if its pores are up to 2nm, mesoporous when the pore diameters are between 2 and 50nm, while the materials having larger pore openings than 50nm are defined as macroporous. [6]

Ultimately, it should be noted that the appearance of faults or defects can affect the crystalline structure of zeolites and, in some cases, completely destroy it.

2.2. Properties and Applications

The most general physical property of zeolites is the existence of a regular microporous system, due to their crystallinity. High thermal and hydrothermal stability allows them to be used as catalysts under severe temperature conditions. [8]

Zeolites can also be used as ion exchangers, due to their capacity to replace the cations in the framework by ions present in external solutions. Ion exchanging zeolites has been widely used to modify the catalytic or sieving actions of the original zeolite. [3]

Moreover, zeolites have a large internal surface area, due to their microporous structure of channels and cavities. Hence, there is a high concentration of active sites inside the framework, whose strength and number can be modified to meet the desired experimental conditions. Since catalytic

reactions over zeolites occur within their intracrystalline cages and channels, the stability, activity and selectivity of all the reactions carried out over zeolite catalysts depend on the shape and size of the cages and channels. Thus shape selectivity is a general characteristic of zeolite catalysed reactions. It is the impossibility of certain molecules entering or exiting the zeolite's pores. [10] The zeolites of a specific pore size on their external surface can allow diffusion of molecules of smaller size or shape into their internal pores. Some cations are too large to enter the internal pores and consequently they are adsorbed in the surface pores of zeolites. [8] Due to the restricted space of the pores, confinement effects may appear, which make zeolites behave like solid solvents. Molecules can be physisorbed in zeolite pores due to this effect, and in a confined and restricted environment the actual concentrations of the reactants are higher than in bulk. [6]

Furthermore, Si/Al ratio is an important parameter, which can influence such adsorption by zeolites. The higher the Si/Al ratio, the smaller the framework charge and the higher the number of water molecules present. [3]

2.3. Acidity

One of the most important properties of zeolites is the surface acidity. In fact, the beginning of the success of zeolite catalysts in industry was due to the replacement of amorphous silica-alumina catalysts by acid Faujasite-type zeolites in fluid catalytic cracking (FFC). [6]

Zeolites can present two types of acidity: Brønsted acidity and Lewis acidity. Furthermore, the ability of a certain species to quicken a reaction by acid catalysis depends on the acid strength of that species as well as their accessibility. In other words, the acid Brønsted strength is the tendency of the acid species to give away a proton so that another species can bond to the acid site.

In Brønsted's view, an acid is defined as a proton donor, whereas in Lewis's theory an acid is an electron acceptor. A Brønsted acid has an extra proton to give to other species, while a Lewis acid has a vacant orbital that can accept a pair of electrons. Ergo, the acidic nature of a zeolite can be described by the characteristics of containing Brønsted and Lewis acid sites. [4]

Brønsted acid sites (figure 3) correspond to bridging OH (hydroxyl) groups linking Si to Al, formed by a proton directly bonded to a framework oxygen atom connecting one Al and one Si atom: Si-O(H)-Al. Initially, the bridged OH group was defined as a silanol group (SiOH) activated by the neighbouring Al^{3+} Lewis acid centre, however it was later considered that the O-Al, O-Si and O-H bonds are all strong covalent bonds covered by small electrostatic interactions. [11]

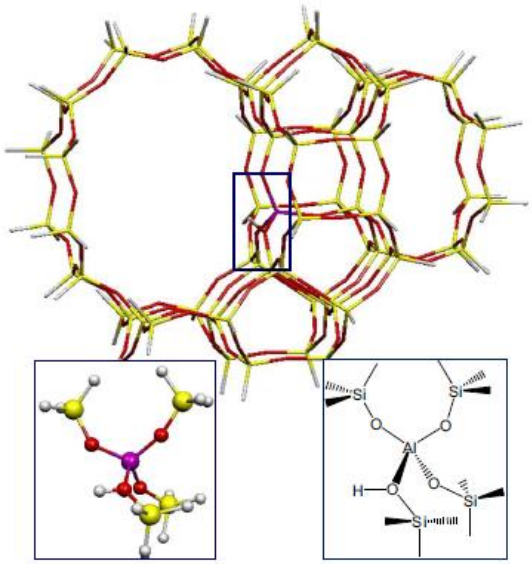

Figure 3 - Brønsted acid sites [10]

It is possible for some of the Si atoms at tetrahedral sites of the zeolite framework to be substituted by Al atoms. Then, the fourfold coordinated Al atom has a negative charge which is balanced by a nearby extra framework cation. [12] Seeing that, in the case where this cation is a proton, a Brønsted acid site is formed, the number of cations depends on the overall charge of the AlO4 tetrahedra. Hence, the maximum number of protons in the acid sites equals the number of framework Al atoms. [3]

The activity of the proton groups depends on their number, acidic strength, accessibility and proximity; given that proton activity is directly proportional to their strength. The T-O-T bond angle is also an important factor: the greater the angle, the higher the acid strength will be (and consequently the T-O bond strength increases and the O-H strength decreases). [4]

Assuming equal structures of bridging OH groups in zeolites in which Al is replaced with different metal atoms (SI-O-H-T), T=Ga, Fe, In, B, etc., the acidic strength of the hydroxyl protons depends on the chemical behaviour of those atoms. [6]

Besides bridging OH groups, there are other types of hydroxyl groups, such as silanol groups (SiOH) and extra-framework Al (EFAL) hydroxyls - AlOH. However, Brønsted's OH groups are much more acidic than silanol's OH groups. Regarding EFAL groups, these are produced by mild steaming leading to partial dealumination, therefore reducing the number of Brønsted sites by converting them into Lewis sites. [13]

Lewis acid sites in zeolites can be due to charge-balancing extra-framework cations (such as Na, K, Cs, Cu, Co, Zn, Ga), extra-framework aluminium species and heteroatoms substituted at framework T position. [13]

The acidity of aluminosilicates depends on the coordination number of aluminium and on the chemical nature of its neighbours. The dehydroxylation of alumina hydrates creates coordinately unsaturated sites (CUS) which are at the origin of the Lewis acidity of these materials. Dehydroxylation, steaming, or dealumination of acid zeolites dislocates aluminium from the lattice into extraframework aluminium. [14] Although Lewis acid sites are not as active as Brønsted sites, they can enhance the strength of Brønsted sites, since water can transform Lewis into Brønsted acidity by dissociative water adsorption, consequently creating M-OH groups. The stronger the acidity of the adsorbate used, the higher the acidity of the generated Brønsted sites. [15] Furthermore, Brønsted and Lewis acid sites can be converted into one another: dehydroxylation of BAS at high temperatures generates LAS. Also, water can transform Lewis into Brønsted acid sites by dissociative water adsorption, consequently forming M-OH acidic groups (figure 4). [4]

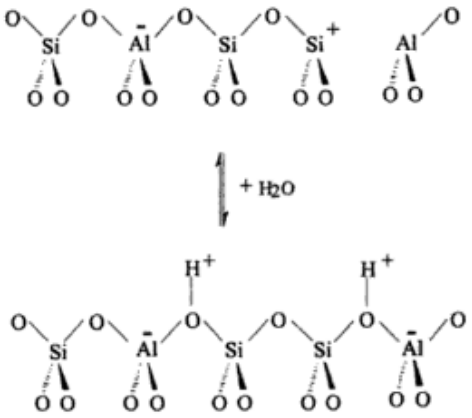

Figure 4 - Water dissociation on Lewis sites to form Brønsted sites [16]

2.4. Basicity

The basic properties of zeolites are much less studied than their acidic properties, due to the fact that industrial heterogeneous catalytic processes using basic catalysts are noticeably less developed than acid catalysed processes. [13]

By the Brønsted-Lowry theory, a base is a proton acceptor, while Lewis states that a base is an electron donor. In zeolites, basic sites are associated to negatively-charged framework oxygen atoms, which is due to the presence of Al in the framework. Moreover, the charge on the oxygen atoms is proportional to the amount of Al in the framework. [13] Besides framework oxygen atoms, other basic sites may be detected in zeolites, such as basic oxygen atoms or hydroxyl groups in oxide clusters or hydroxyl groups originating from water dissociation in hydrated extraframework cations.

To analyse the basicity of zeolites, one must determine the number and strength of those basic centres. The most widely used approach is the use of acid probe molecules that would react with the basic sites, and characterizing them by IR spectroscopy.

Sanderson postulated a principle for equalization of electronegativities for framework atoms in zeolites, calculating the mean electronegativity of the zeolite framework by the geometric average of the

electronegativities of all atoms contributing to the framework. Using Sanderson's principle, the charge on the framework atoms and cations in zeolites can be estimated. [6] The higher the framework aluminium content, the higher the basicity of the framework oxygen atoms, because comparing to silicon, aluminium has lower electronegativity. Given that, zeolites are usually used as basic catalysts in their alkali-exchanged or impregnated forms. [6]

Decreasing the T-O-T bond, increasing aluminium content or increasing the T-O-T bond length is known to improve the basicity of a zeolite, since it influences the negative charge on the oxygen atoms.

2.5. Zeolite Y

Zeolite Y (figure 5) is a synthetic Faujasite introduced for the first time on an industrial scale in Fluid catalytic Cracking (FCC) of heavy petroleum distillates in 1962. They were more active and granted a meaningful increase in the gasoline yield, which is the most valuable of oil products. Furthermore, it has been estimated that the cost of oil refining would be higher by at least 10 billion US dollars per year if zeolite catalysts wouldn't be used today. [17]

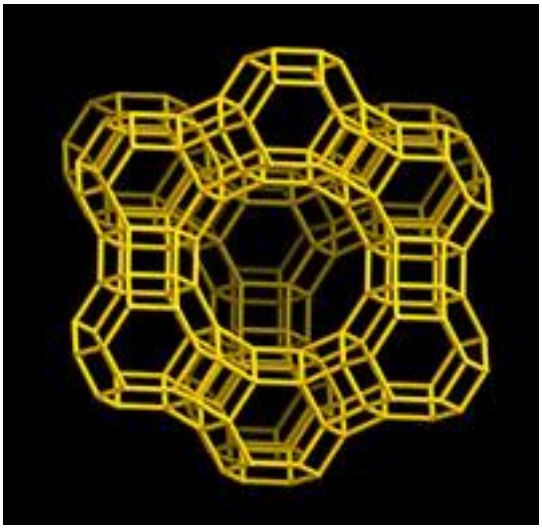

Figure 5 – Zeolite Y unit cell structure [International Zeolite Association – IZA]

Its pore system comprises spherical cages, most commonly called supercages, with 1,3 nm in diameter. These supercages are connected with four neighbouring cages, through pores with 0,74 nm

in diameter, through windows formed by TO_4-tetrahedra. Hence, it is said that Zeolite Y has a three-dimensional 12-membered ring pore system, as it can be seen in figure 6. [17]

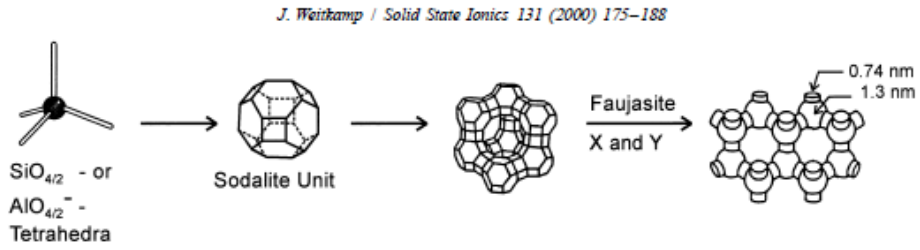

Figure 6 - Structure of zeolite Y [17]

Even though zeolite Y's thermal and hydrothermal stability is acceptable, it is rather limited. Given that the increasing the Si/Al ratio increases the stability; dealumination of the framework by addition of steam was developed, as a way to produce ultra-stable zeolite Y (USY). By removing aluminium from the framework, it changes the catalytic activity, since extra-framework Al stabilizes the lattice. Dealumination is a way of increasing the acid strength of the protons remaining in the structure. As it was mentioned previously, the number of Brønsted acid sites is related with the number of framework Al species. Therefore, catalytic activity increases with the number of Brønsted acid sites. [18]

Due to Zeolite Y's shape selectivity, the diffusion of compounds in its pores and the size of molecules that can be catalysed are somewhat limited. The strategy used to improve this situation was the creation of mesopores.

There are two main approaches: top-down techniques (that involve removal of Silica or Alumina) and bottom-up techniques that use soft or hard templates. Ultrastabilization of Ammonium-ion-exchanged zeolite Y in order to create USY is an example of a top-down process. [19]

The extra pore volume obtained with the creation of mesopores in the zeolite and surface area serve as a positive support for the catalyst particles that provide hydrogenation function of the bi-functional hydrocracking catalyst. [20]

The creation of mesopores in zeolite Y gives rise to the concept of hierarchical zeolite structures. Hierarchical zeolite is a zeolite that contains two or more types of pores of different size, thus a mesoporous zeolite should be considered a hierarchical zeolite, since it has a secondary pore-structure system in the mesopores range (2-50nm). [20]

The Zeolite Y used in this work has a global Si/Al ratio of 2,6 and was acquired from CROSFIELD. This material did not have any mesopores.

2.6. Characterization

The catalytic activity of a zeolite is defined by its properties, such as: structure of the zeolite, size and shape of its pores, composition, texture, acidity, morphology. To accurately characterize all these properties, several characterization techniques were used.

The experimental techniques used to characterize the zeolites are compiled in the table 1.

Table 1 - Experimental Techniques used in this work

Property	Characterization Technique
Structure (crystallinity)	X-Ray Diffraction (XRD)
Acidity	Infrared Spectroscopy (IR)
Texture and pore size	Physical Adsorption (N2)
Morphology	Scanning Electron Microscopy (SEM)

In this work, the goal was to produce a mesoporous zeolite Y, for further use in biodiesel catalysis. To achieve that, several treatments were made, with different amounts of citric acid in the mesoporous treatment and with different sequences (it was experimented which route was better: if ion exchanging zeolite NaY to NH_4Y and then creating mesopores or the other way around).

After all samples were prepared, they were characterized using the techniques mentioned above, being that IR spectroscopy was done using two different approaches: Pyridine adsorption to quantify the acid sites, and different probe molecules to distinguish between internal and external pores.

This work was developed in the Birchall Centre, located in the Lennard-Jones Laboratories, at Keele University, Staffordshire, United Kingdom.

3. Experimental Techniques

3.1. Modification Techniques

To obtain an improved zeolite Y, various modifications were made. The modification techniques used in this work were Ion Exchange, Surfactant Templated 'top-down' approaches (in order to create mesopores) and calcination.

3.1.1. Ion Exchange

In an Ion Exchange, an excess volume of solution is added to the zeolite support, under stirring conditions, over a period of time so that the ions in the solution progressively replace the ions in the zeolite's pores. [21] Afterwards, the mixture is washed and centrifuged in order to remove the excess solution and left to dry.

In the particular case of this work, zeolite NaY was ion exchanged with ammonium hydroxide and ammonium acetate, to replace Na^+ ions by NH_4^+ ions. Since only about 73% of Na^+ ions can be exchanged in a single ion exchange [21], several repetitions of the operation are necessary to exchange all sodium ions.

The procedure was carried out using a dissolution ratio of 1/10 (20g of zeolite mixed in 200mL of a solution of 0,1 M NH_4NO_3/NH_4CH_3COO). The mixture was stirred at 80 °C for 1 hour, centrifuged at 4250 rpm for 12 min to separate the solid product, which was then washed with H_2O. The procedure was repeated 3 times to increase the degree of the exchange. Afterwards, the samples were dried overnight in an oven at 40°C.

Two samples were prepared: using NH_4NO_3 and NH_4CH_3COO (see Table 2).

Table 2 -Ion Exchanged samples

Zeolite	Solvent	Concentration	Sample name
NaY	NH_4NO_3	0,1 M	$NH_4Y(NO_3)$
	NH_4CH_3COO	0,1 M	$NH_4Y(OAc)$

3.1.2. Mesoporous Surfactant Templated Treatment

In order to create mesoporous in Zeolite Y, a 'top-down' procedure was used. This approach is a destructive approach, which can sometimes lead to loss of crystallinity. The ultra-stabilization of ammonium ion-exchanged zeolite Y by dealumination by heating the NH_4Y causes the hydrolysis of the Al-O-Si bonds and consequently the expulsion of Al from the framework. Some of the vacancies left by Al atoms are filled with Si atoms and others merge to form larger cavities (mesopores). However, this method was proven to be insufficiently efficient, since the mesopores were in fact cavities entrapped in the zeolite's crystals. The Surfactant Templated treatment consists of hydrothermal treatment with a cationic surfactant, citric acid and a basic solution (NH_4OH in this case). It has the advantaged of introducing mesoporosity without significantly compromising the Si/Al ratio or the pore distribution of the zeolite.

USY zeolite with Si/Al= 2,5 was the starting material for this experience. 5g of zeolite were dissolved in 50 mL of deionized water and stirred. Citric acid 10% (m/m) was added in 4 times, each one left to stir for 15 minutes. After the 4 additions, the sample was centrifuged, washed and left to dry in open air for 1 hour. Afterwards 50 mL of H_2O were added to the sample, followed by 2,5 g of cationic surfactant (CTABr - Cetyltrimethylammonium bromide) and 10 mL of Ammonium Hydroxide (35%). After mixing well, the resulting mixture was left in an over at 80 °C for 24 hours.

The cationic surfactant is very important in this procedure, because it introduces mesoporosity and protects the zeolite's structure from citric acid, since it dissolves aluminium ions. Also, it allows for a much higher hierarchy factor and more efficient microporosity preservation. [19] The proportion of surfactant/zeolite should always be ½, which is half of the zeolite amount is the optimum amount of surfactant. This was verified by previous work at Lennard-Jones building at Keele University.

After the drying process, the sample is centrifuged and washed with H_2O, followed by calcination. The calcination programme used is the following (figure 7):

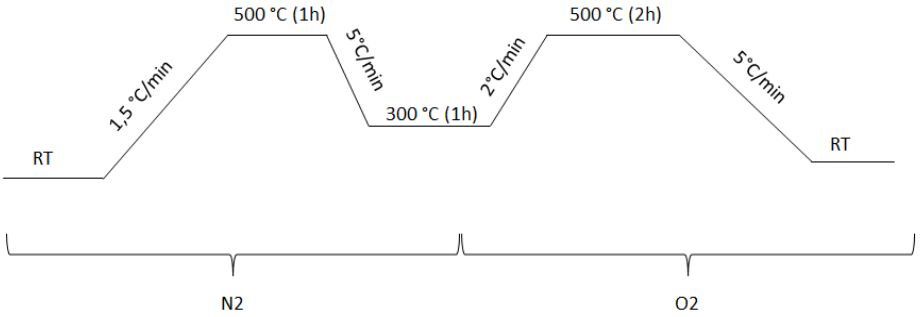

Figure 7 - Calcination programme used in zeolite samples

The maximum temperature for this type of zeolite is 500°C, instead of 550°C [22], otherwise the sample is partially destroyed. This was verified by previous work at Lennard-Jones building at Keele University.

This procedure was done with different amounts of citric acid, in order do decide which one gave the best results. The amount of citric acid was calculated in milliequivalents, for 5 g of zeolite.

Table 3 -Samples prepared with different amounts of citric acid

Amount of zeolite (g)	Amount of citric acid (meq)	Amount of citric acid (g)	Sample name
5g	1,5 meq	4,80 g	1.5 USY
	3,0 meq	9,61 g	3.0 USY
	4,5 meq	14,4 g	4.5 USY
	6,0 meq	19,21 g	6.0 USY

3.1.3. Calcination

Calcination is a thermal treatment that affects the physico-chemical properties of heterogeneous catalysts and enhances its activity. [23] This treatment was only applied to one of the samples (NH_4Y 6 IE calcined), because it was verified that it became amorphous due to this thermal treatment. The calcination programme used was the following (figure 8):

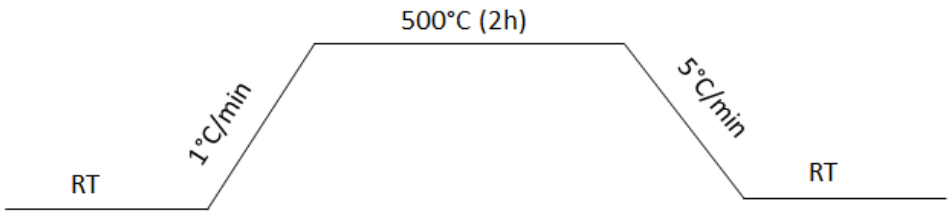

Figure 8 - Calcination programme used for sample "NH4Y 6IE calcined"

In this work, 6 samples were prepared, with different properties and different amounts of citric acid, in order to find out which one is the optimum preparation method. The original zeolites as made by the respective companies were also characterized for comparison and as a way to validate the results obtained.

Two different routes were in study: Route 1 and Route 2. Route 1 consists of ion exchanging NaY to NH4Y first, and then treat it with citric acid, while Route 2 is treating NaY with citric acid, and then ion exchange it to NH4Y.

The samples were labelled as follows:

Table 4 -Summary of the samples prepared

Sample name	Sample nr	Description
NH4Y IE	1	Starting material: NaY from Zeolyst Sample was ion exchanged 4 times with NH_4NO_3 and NH_4CH_3COO. Two samples resulted but were treated as only one, since their properties were the same.
NH4Y 6	2	Starting material: NH4Y IE After the ion exchange, sample received mesoporous templated surfactant treatment with 6 meq citric acid
NH4Y 6 calcined	3	Starting material: NH4Y IE

		After the ion exchange, sample was calcined and then received mesoporous templated surfactant treatment with 6 meq citric acid
NH4Y 4.5	4	Starting material: NH4Y IE After the ion exchange, sample received mesoporous templated surfactant treatment with 4.5 meq citric acid
NaY 6	5	Starting material: NaY from Zeolyst Sample received mesoporous templated surfactant treatment with 6 meq citric acid and then was ion exchanged with NH_4CH_3COO.
NaY 4.5	6	Starting material: NaY from Zeolyst Sample received mesoporous templated surfactant treatment with 4.5 meq citric acid and then was ion exchanged with NH_4CH_3COO.
Original NaY		NaY from Zeolyst
Original NH4Y		NH4Y from CROSFIELD

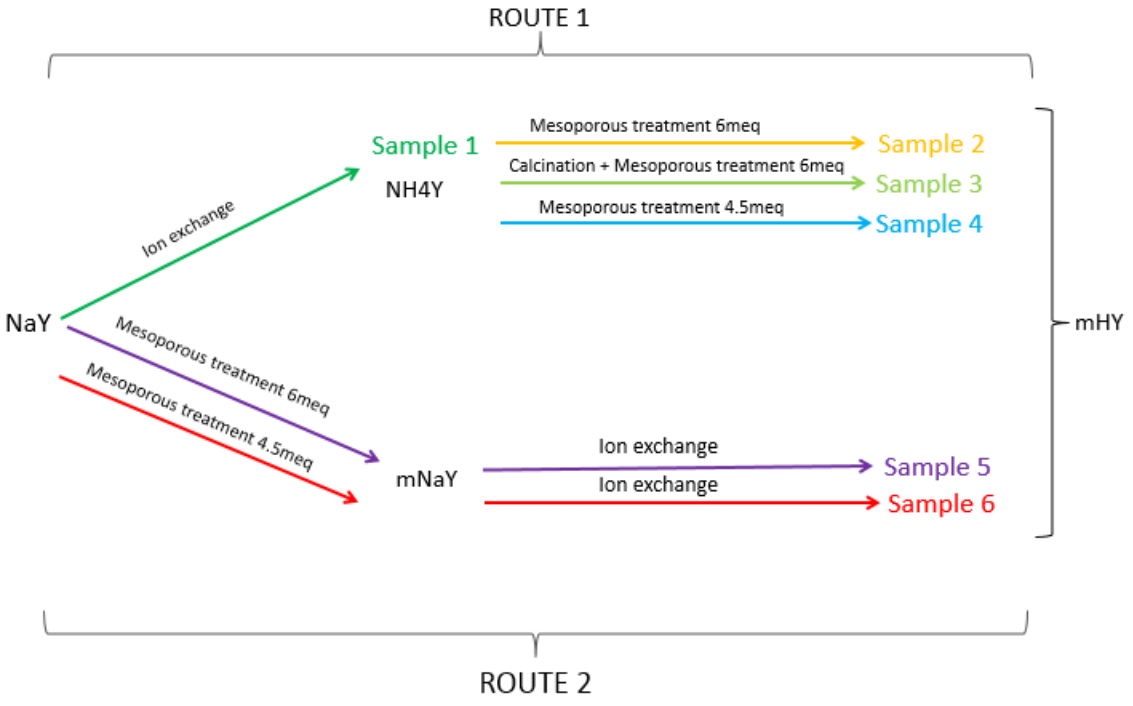

Figure 9 - Diagram showing the different routes and the different treatments received by the samples

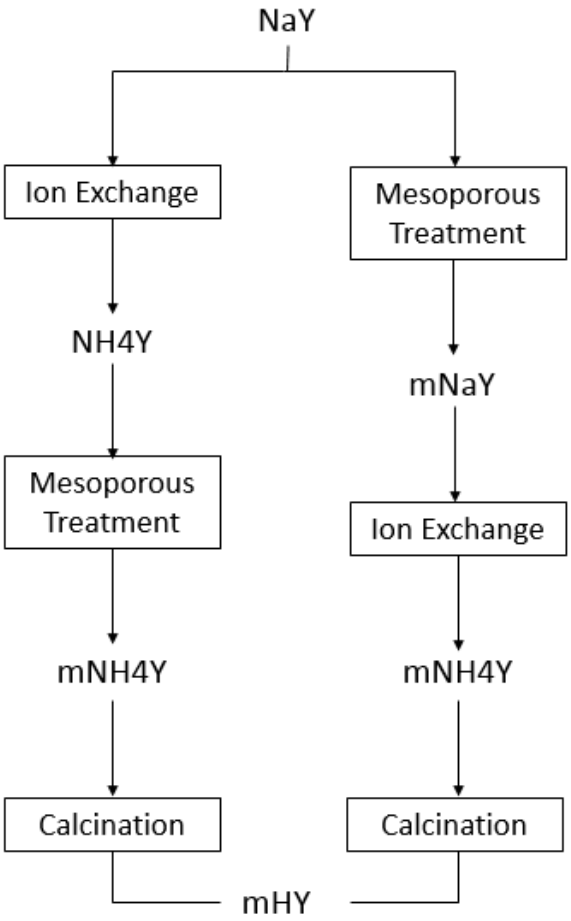

Figure 10 - Block diagram of the operations used in this work

3.2. Characterization Techniques

3.2.1. Sorption Analysis

Gas adsorption is very important for the characterisation of a wide range of porous materials, since it allows the measurement of the specific surface area of materials, the pore size, volume and distribution. The probing gases more often used are Argon, Krypton and Nitrogen at 77 K. [24]

Adsorption is a general phenomenon which occurs when a gas or liquid (fluid) comes in contact with a solid. The fluid is retained by the superficial atoms of the solid and fixed at the solid surface. In the Sorption experiments, the gas released into the sample holder is called adsorptive, the solid on which the adsorption occurs is known as adsorbent and the adsorbed phase is named the adsorbate. [24] Evidently, desorption indicates the liberation of fluid retained by adsorption on the solid surface.

As the gas amount increases, the surface becomes progressively covered with adsorbate until a monolayer is formed, covering the entire porous surface. After that, increasing gas quantities will lead to the formation of multilayers until the pores are totally filled with gas. The equipment used for the sorption experiments is shown in figure 11.

Adsorption measurements can be carried out using different methods. The most common ones are the volumetric and gravimetric methods. The adsorption measurement consists of administering a known amount of adsorptive gas into the reference volume (V_{ref}). Then, the reference volume is opened to the sample volume (V_{sample}) until equilibrium between the sample and the gas is achieved. [24]

Figure 11 - Equipment used for the sorption experiments (*Quantachrome Autosorb C1*)

The main focus points are pore size and volume. Regarding pore size, solids with pore openings from 0.4 to 2 nm are called micropores, whereas mesopores have pore widths from 2 to 50 nm. According to IUPAC, the amount adsorbed per gram of adsorbent as a function of the relative equilibrium pressure (P/P_0 where P is the equilibrium pressure and P_0 refers to the saturation vapour pressure at the adsorption temperature) is called an isotherm. There are six types of isotherms (I to VI), which can be found in figure 12. [24]

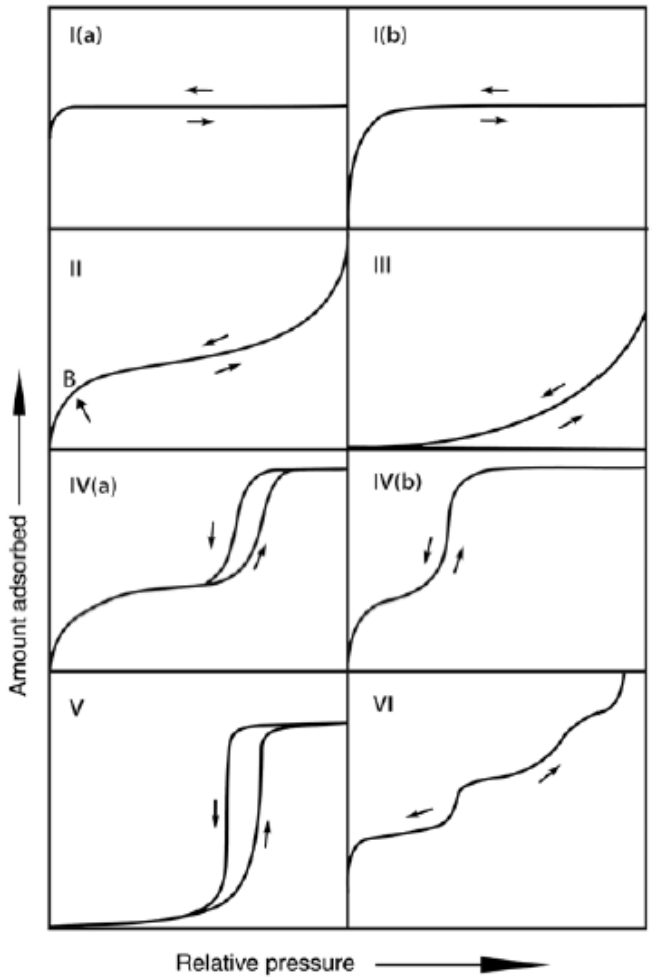

Figure 12 - Isotherms (I to VI) defined by IUPAC [25]

It should be noted that each isotherm is characteristic of the adsorbate-adsorbent duo to be analysed. Thus, one should consider singularities such as gas polarity or solid surface chemistry.

Type I isotherms, also known as Langmuir isotherms, are given by microporous materials having small external surfaces. Type II isotherms are given by the physisorption of the gas on nonporous or macroporous adsorbents. If the 'elbow' is sharp (point B), it corresponds to the completion of the monolayer formation. If there is as more gradual curve, it means that there is a significant amount of monolayer coverage, hence leading to the formation of a multilayer. In type III isotherms, the adsorbent-adsorbate interactions are weaker and the adsorbed molecules are aggregated on the best surface sites of a nonporous or macroporous solid. If there are mesopores, the initial monolayer-multilayer adsorption on the mesopores walls is followed by pore condensation, being represented by type IV isotherms. In

case of hysteresis, when the pore width exceeds a certain width (critical width), the curve obtained is type IV(a). Type V isotherms are observed for water adsorption on hydrophobic microporous and mesoporous adsorbents. In type VI isotherms, one can observe layer-by-layer reversible adsorption on a nonporous surface. [25]

IUPAC also considers four limiting cases for hysteresis loops (H1 to H4), which are associated with capillary condensation in mesopores (figure 13). Pore condensation is the phenomenon through which a gas condenses to a liquid-phase in a pore at a pressure (p) smaller than the saturation pressure (p0). [25]

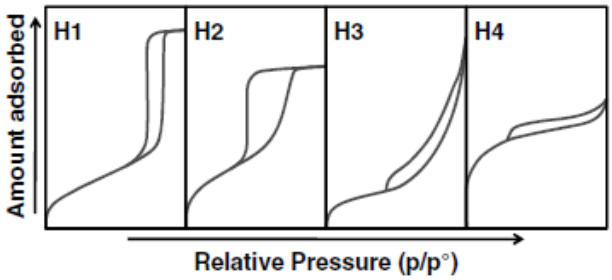

Figure 13 - Hysteresis loops (1 to 4) described by IUPAC [25]

Type H1 loop is associated with adsorption in unconnected mesopores with a tight pore size distribution, while hysteresis type H2 is mostly due to pores which are interconnected. Type H3 loop is due to non-rigid pore structures between particle grains and H4 is associated with non-rigid pore structures between flat plates. [24]

The BET equation, proposed by Brunauer–Emmett–Teller in 1938, is based in the assumption of multilayer adsorption, being an extension of the Langmuir theory for monolayer adsorption. This equation is frequently used to evaluate the specific surface area of materials. It is based on the assumption of multilayer adsorption on a flat surface and it is used for adsorption on mesoporous solids. The BET method for evaluating the surface area is accepted as standard, so, even though it cannot be

used in microporous solids, it is possible to apply the BET method obtaining an *apparent* surface area that can be used as an adsorbent “fingerprint”. [24]

Before the determination of an isotherm, all the physisorbed species need to be removed from the surface of the adsorbent, thus the need to do the outgassing of the adsorbent (exposure of the surface to high vacuum at high temperature). The weighed sample (22-27 mg) is placed in the sample holder (a 12 mm bulb cell), which is loaded into the outgasser station. The outgassing is run overnight, according to the scheme below (figure 14). After this, the sample is left to cool down naturally and then degassing. Afterwards, the sample is transferred to the sorption station and the sorption experiment begins: a Dewar container filled with liquid nitrogen starts to rise towards the sample, after 30-40 min, so that the sample is placed in cryostat bath. After 30 minutes, the Dewar starts to drop and the adsorption data points appear. The program used to run the analysis is called *Quantachrome ASiQwin 3.0*. Multi-point BET (Brunauer–Emmett–Teller) theory was used to calculate the surface area, DTF (density functional theory) used to determine pore size distribution and diameter and *t-plot* method to evaluate micropore volume and external surface area. [24] [25]

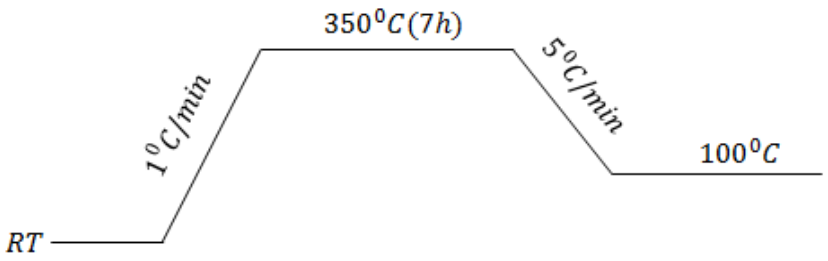

Figure 14 - Activation programme used in the sorption experiments

3.2.2. X-ray diffraction (XRD)

X-ray powder diffraction is a very important way to determine the structure and crystallinity of a crystalline material. Irradiation of X-ray in zeolite powders (1-50μm diameter) produces a scattering

pattern that reflects the framework topology and the positions of extra-framework cations and/or adsorbed molecules. These powder diffraction patterns serve as the “fingerprint” of the material. [26]

An X-ray diffractometer consists on an X-ray source, a sample and a detector (known as Bragg-Brentano detector – figure 16), which are all in the same plane during the experiment, wherein the detector moves on a single dimension and records intensity for each 2θ angle (figure 15). [26]

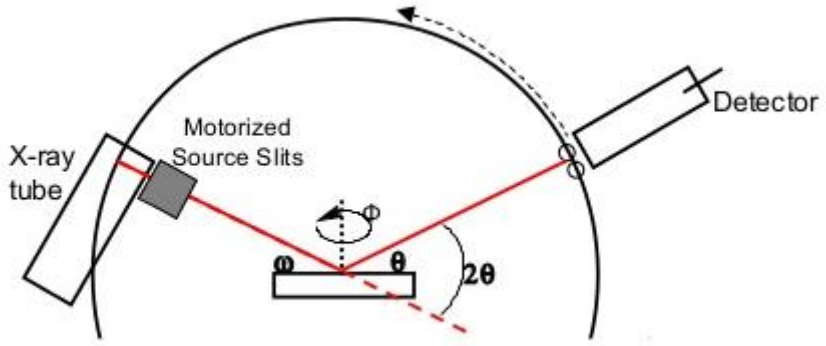

Figure 15 - Incident x-ray source and detector angles [27]

The incident radiation angle (ω) is always half of the detector angle (2Θ), since it is between the source and the sample. The detector angle, on the other hand, is between the incident beam and the detector.

When monochromatic radiation (x-rays) of wavelength λ strikes parallel crystal planes (in polycrystalline samples) separated by an interplanar space (d), constructive or destructive interference occurs. Constructive interference occurs when the angle θ between the plane and the x-ray results in a path-length difference that is an integer, n, multiple of the x-ray wavelength (λ). This can be translated into the Bragg’s Law: [6]

$$n\lambda = 2d\ sin\theta$$

In a powder diffraction experiment, a particular reflection will yield a ring of diffracted intensity at an angle 2θ because of the random orientation of the crystallites, while in a single crystal diffraction experiment the reflection will yield a discrete diffraction spot. [28]

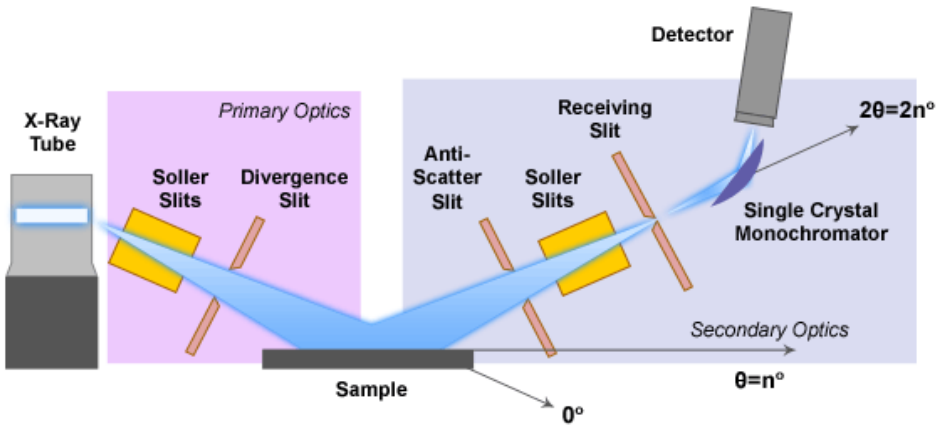

Figure 16 - Scheme of a Bragg-Brentano diffractometer [29]

The results given by the diffractometer are plots of intensity vs 2θ, as shown in figure 17.

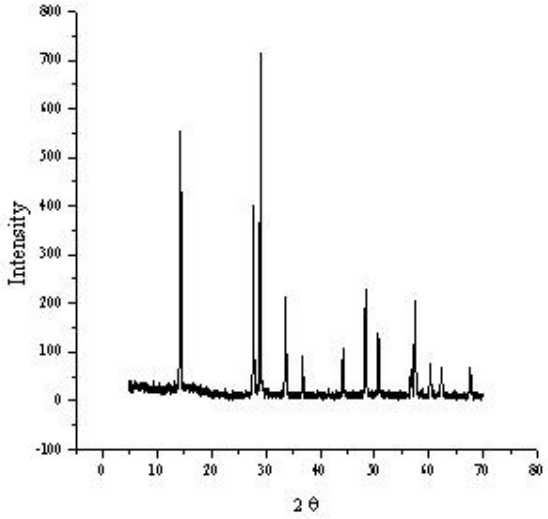

Figure 17 - XRD diffraction plot [30]

Given that atomic dimensions are of the same magnitude as the wavelengths of X-rays and that electrons are distributed all over the volume of the atom, X-rays scattered from different regions do not scatter in phase. Hence, there is partial interference from electron density in different regions of the same atom, which leads to a reduction of the scattered amplitude of the atom. [26]

After collection of the diffraction data, the patterns can be compared with reference patterns for a determined material or profile functions can be fitted to the experimental pattern peaks, to obtain the 2θ reflection positions. [26]

Regarding sample preparation, the powdered sample is deposited and spread over a diffraction plate. Then it was loaded onto the sample holder of the XRD machine, after which the experimental parameters are set and the programme is started.

Another useful use of X-ray diffraction is the determination of the zeolite's unit cell size, given that it allows the calculation of the Si/Al ratio in the framework. In a crystal, each lattice point can be related to another by a number of translations in the a,b,c directions. These vectors a,b and c comprise a volume called a unit cell. [26]

The lattice points of a determined structure describe an infinite number of parallel planes. The three-value Miller index notation is commonly used to describe vectors and planes in a crystal lattice, using the indices [*h k l*] as directional parameters. [26] These lattice planes are relevant in diffraction studies because the diffraction from a batch of lattice points is equivalent to reflection from these planes. Therefore, each [hkl] set of planes leads to a potential diffraction maximum at a diffraction angle (θ) described by Bragg's law. [6]

By mixing silicon with the powdered zeolite (in a proportion of 1 g of zeolite to 50 mg of silicon) and collect the resulting diffraction patterns it is possible to calculate the unit cell size of a given zeolite. The procedure followed a *Standard Test Method for Determination of the Unit Cell Dimension* [28]: the first step is blending 0,5 g of zeolite with 0,025 g of silicon and leaving the mixture in a hydrator for 16 hours. Afterwards, the sample preparation procedure is the same as mentioned before.

The equipment used was a *Bruker D8 Advance* with nickel filtered CuKα radiation. The patterns were scanned in a 2θ range between 5–60°, with a coupled 2θ/θ scan type, at an angular rate of 0,3°/min and a 0.01° step.

3.2.3. Infrared Spectroscopy (IR)

This technique can give information on the functional groups, bonding types and nature of the compounds to be analysed. The adsorption band in an IR spectrum only appears in molecules whose vibrations correspond to a variation in the dipole moment.

Infrared Spectroscopy (IR) is one of the most broadly used techniques, since it gives information on zeolite formation, framework vibrations, surface property, adsorption and catalysis. [32] The most widely used spectrometer is a FTIR (Fourier Transformation Infrared) type, which consists of a source, Michelson interferometer, sample compartment, detector, amplifier, A/D converter, and a computer. [33]

The basic working principle of this type of spectrometer is that the signal collected is amplified and converted to digital signal and then converted into spectra via Fourier transform.

The core of FTIR spectrometers is the Michelson interferometer (figure 18) that is a device that produces interference between to beams of light, consists of two perpendicular mirrors and a beamsplitter. One of the mirrors is stationary and the other is a movable mirror. The beamsplitter (usually made of KBr or CaF_2) splits the beam of light coming from the source into two parts. One part of the light travels a different path length than the other. After traversing these different path lengths, the two parts of the light are brought together to interfere with each other. The recombined beams are then sent into the detector, which measures the difference of intensity of these two beams as a function of the difference of the paths. The resulting interferogram is then transformed into a spectrum of intensity as a function of the wavelength, via a Fourier transform (figure 19). [34]

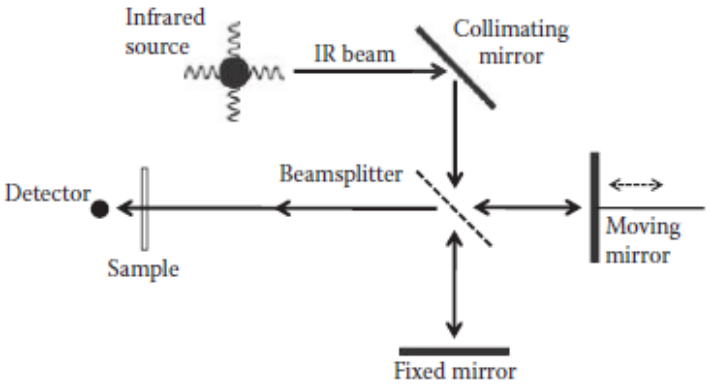

Figure 18 - Michaelson Interferometer scheme

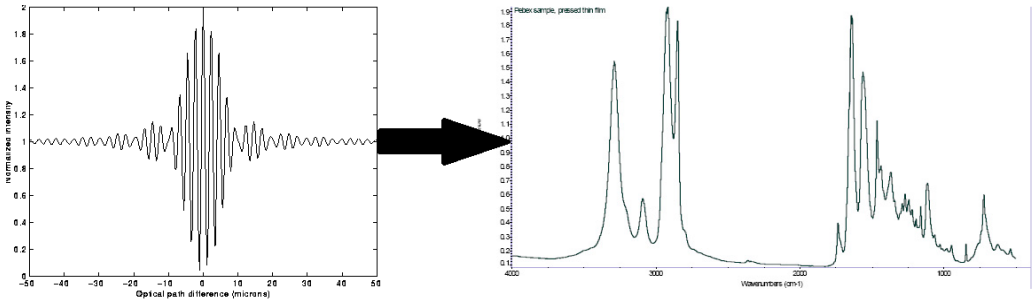

Figure 19 - Interferometer to spectra transformation

When the two beams recombine, if the position of the moving mirror is such that the reflected beam is in phase with the fixed mirror, they produce a constructive interference that translates in a peak in the interferogram. If the recombined beams are out of phase, they produce a destructive interference; therefore no peak will appear in the interferometer. [35]

To produce an interferogram, the mirror is moved back and forth once – this is called a scan. The higher the number of scans, the smaller the noise in the final spectrum and better will be the quality of the spectrum. [35]

The obtained spectrum plots absorbance (A, a.u.) as a function of wavenumber (v cm^{-1}) wherein with the wavenumber being presented from higher to lower values, by convention.

IR spectroscopy is arbitrarily divided into three categories: near-IR (> 3000 cm^{-1}), mid-IR (4000-400 cm^{-1}) and far-IR (< 300 cm^{-1}). For zeolite studies, mid-IR is the best region since it provides information on surface OH groups, adsorbed molecules and framework vibrations. [31] IR spectroscopy allows to study the type, concentration and acid strength of OH groups in zeolites. The band position of the OH groups depends on the type of zeolite, the framework Si/Al ratio, type of coordination of the oxygen (terminal or bridging), the disturbance of the OH group through the surroundings by lattice or extra-lattice oxygen and the co-existence of other cations. [6]

If the oxygen of a hydroxyl group is connected to more than one cation, it is called a Bridging OH group (M1-(OH)-M2). Those bridging OH groups appear at lower wavenumbers due to the M-O bond order in bridging hydroxyls is half of the M-O bond order in M-OH hydroxyls. Bridging OH groups are located in the zeolite pores, whereas silanol groups are located mostly on the external surface. [36]

Theoretically, the higher the acid strength of the bridging OH group, the weaker is the O-H bond, ergo the lower is the stretching frequency. Besides, the T-O-T bond angle (T being Si or Al) relates to the acid strength: the greater the angle, the higher the acid strength. The typical values of the O-H stretching wavenumber vibrations are presented in table 5: [4]

Table 5 -Typical values of the OH stretching vibrations in zeolites

Hydroxyl group	Vibration wavenumber range (cm^{-1})
Bridging acid sites	3600–3650
Terminal silanol	3745–3750
Internal silanol	3700–3720 (isolated)
	~ 3500 (involved in hydrogen bonds)

Brønsted acid sites can be investigated with and without probe molecules using IR spectroscopy while Lewis acid sites can only be studied with the help of probe molecules. By analysing the spectra, one can distinguish between Brønsted and Lewis sites. The most widely used probe molecules are CO, acetonitrile, pyridine and ammonia. [4] However, since the probe molecule generates a perturbation of the catalyst's surface, the best probe molecule to be used is the reactant itself, because it provides the

same perturbation as during the chemical reaction. [15] By investigating the adsorption and desorption of probe molecules it is possible to determine the strength, location, nature and amount of these active sites.

The adsorption of pyridine can be very useful, since it interacts with Brønsted acid sites forming PyH^+ (pyridinium ion), and also adsorbs onto Lewis acid sites giving specific adsorption bands in the spectrum (figure 21). Moreover, pyridine probe can differentiate Lewis acid sites with different strengths. Besides, pyridine is thermally stable at high temperatures. [32]

The combination of pyridine with other molecules is useful to differentiate between the acid sites located and large and small cages, since the smaller cages can only be accessed by smaller probe molecules.

Depending on the coordination of the hydrogen atom, surface OH groups can by divided in isolated OH groups and H-bonded OH groups. [36] The main OH groups fond in zeolites are the following (figure 20):

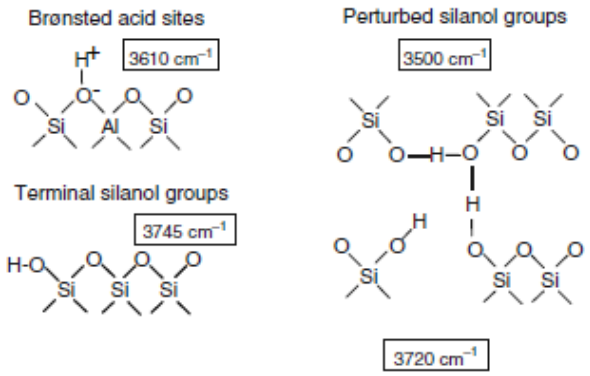

Figure 20 - Types of hydroxyl surface groups present in zeolites and their stretching frequencies [6]

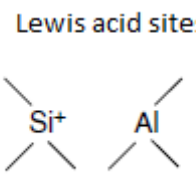

Figure 21 - Lewis acid sites present in zeolites [6]

It should be noted that accessibility depends on the experimental conditions, since the size of the pores depends on the temperature. Some pores may be partially blocked by amorphous material, thus dealumination or desilication of zeolites aids access to OH groups. [36]

One of the most common techniques used in IR is pyridine adsorption. In zeolite Y there are two main OH groups: high-frequency (HF) hydroxyls, located in the supercages and low-frequency (LF) OH groups located in the small sodalite cages. HF hydroxyls have a band around 3650-3625 cm^{-1} and LF hydroxyls appear at 3550 cm^{-1} (figure 22). When pyridine is adsorbed, Brønsted sites are observed around 1540 cm^{-1} and Lewis sites appear at 1450 cm^{-1} (figure 23).

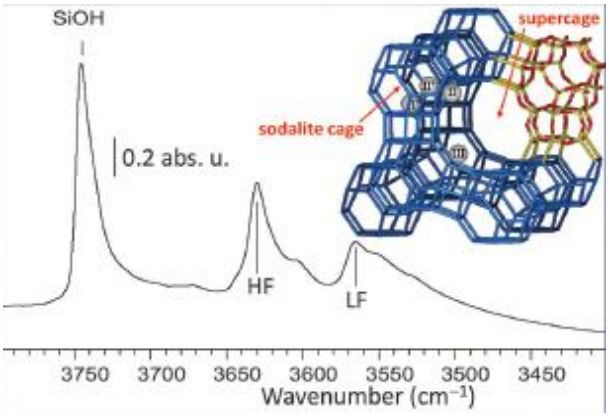

Figure 22 - Stretching frequencies of HF and LF hydroxyls and Silanols [13]

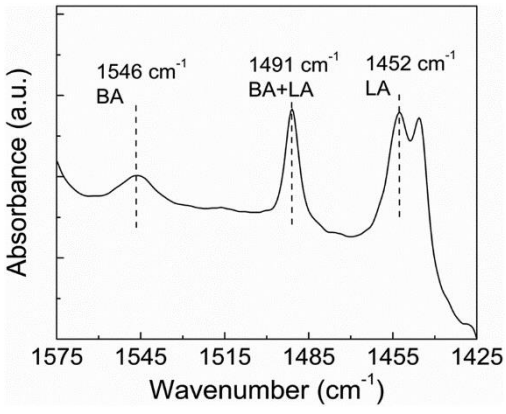

Figure 23 - Typical stretching frequencies of Brønsted (BA) and Lewis (LA) acid sites

Given that IR is a very sensitive technique for detecting impurities (such as water, carbonates, organics and other residual species) it is necessary a previous surface activation of the zeolites. The

activation consists of increasing the temperature up to 450ºC which removes impurities and molecularly adsorbed water, according to figure 24. [15]

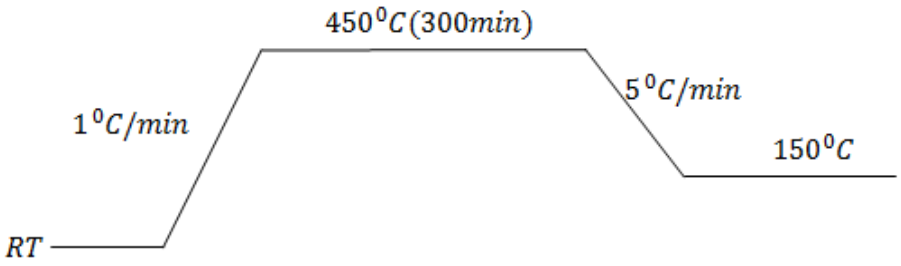

Figure 24 - Activation programme used in the IR experiments

Two different types of experiments were made using the IR spectroscopy: using pyridine adsorption to quantify the acid sites in zeolite Y (both Brønsted and Lewis) and using different probe molecules to distinguish between external and internal pores, by blocking the internal sites with the first molecule, followed by adsorption of a different probe molecule to quantify the external acid sites and so distinguish between micro and mesopores. The molecules used to test the accessibility of the micro and mesopores were nonane (C_9H_{20}), tri-isopropylbenzene ($C_6H_3[CH(CH_3)_2]_3$), deuterated acetonitrile (CD_3CN), di-ter-butil-pyridine ($C_{13}H_{21}N$) and carbon monoxide (CO).

Sample preparation and loading was the same for all probe molecules with the exception of CO. The samples were pressed at roughly 0,5 ton into a pellet holder and loaded into the IR cell, which was opened to atmospheric pressure and disconnected from electric cables, so that the upper part containing the sample holder was removed from the system. After the sample was loaded into the system, the upper part was reconnected as well as the electric cables and the system was then closed and pressurized. Regarding the CO probe, the CO was loaded in the gas flask before the sample and liquid nitrogen was introduced underneath the gas flask in order to freeze the residual CO_2 existing inside, preventing it from going into the system. This is possible because the melting point of CO_2 is lower than CO's melting point, and it was verified in the IR spectra that without the use of liquid nitrogen, the system

and the sample were contaminated by CO_2. In all experiences using the CO probe, the amount used was approximately 7,5 torr.

For the pyridine experiments, the activation programme was run overnight and the system was purged with N_2 (roughly 2 hours before the data collection started). The background spectrum was collected, followed by the spectrum before injecting pyridine. An excess volume of 2 µL of pyridine was injected in the system, to guarantee that all sites were covered. After a few minutes, the excess and physisorbed species was removed by pressure gradient. Then, the desorption programme followed the scheme in figure 25.

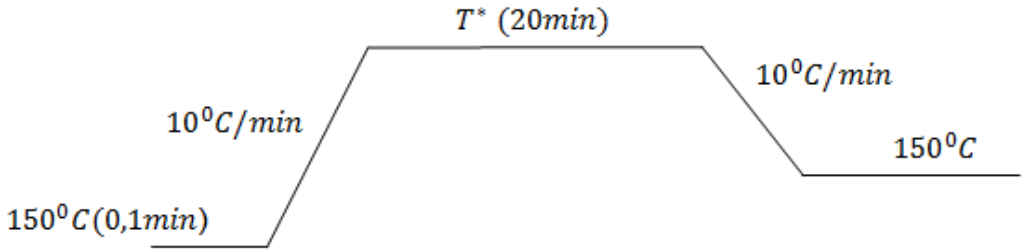

Figure 25 - Pyridine desorption programme used in the IR experiments (T^*= 200,250,300,350,400,450 ^{0}C)

For the different probe molecules used to test the accessibility, the heating was turned off after the activation programme was complete and the sample was left to cool down to room temperature. The C_9H_{20} experiments were made in increments, first 1 µL and then it was added 2 µL at a time, in order to evaluate the necessary amount to cover all the sites. It was adsorbed a total of 10 µL, and then desorbed at room temperature, followed by different temperatures as shown in figure 26.

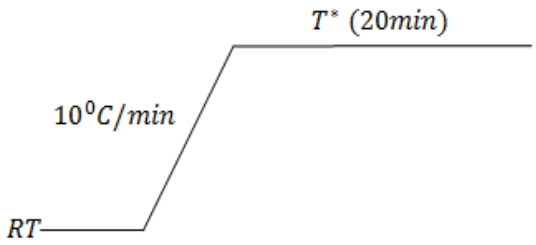

Figure 26 - Desorption programme used in the C_9H_{20} experiments (T=50,70,100,150,200^{0}C)

Regarding CD_3CN, 2 μL were injected into the system, and removed after a few minutes. It was desorbed for 20 minutes at 100 ^{0}C and afterwards the zeolite sample was reactivated at 300 ^{0}C for 1 hour to remove all the remaining CD_3CN. 2 μL of C_9H_{20} were injected to cover all the internal sites, desorbed at 50 ^{0}C for 20 minutes and then 2 μL of CD_3CN were injected and subsequently desorbed at room temperature.

The $C_{13}H_{21}N$ experiments were made in the same way as the previous ones, with the exception of the temperature: it was left at 150 ^{0}C after the activation programme was finished. 1 μL of $C_{13}H_{21}N$ was injected, the pressure was checked, and another 1 μL was injected in order to make sure that it was an excess $C_{13}H_{21}N$, meaning all the sites were covered. It was desorbed at 150 ^{0}C after a few minutes.

Another probe molecule used was $C_6H_3[CH(CH_3)_2]_3$. It was injected 1 μL, the pressure gauge was checked, and one more μL was added to the system, to ensure an excess $C_6H_3[CH(CH_3)_2]_3$. Afterwards it was desorbed at room temperature, followed by different temperatures, as presented in figure 26, being that T=50, 100^{0}C.

Finally, for the CO experiment, it was added roughly 10 torr to the system, the excess was desorbed, and the CO in the gas phase spectrum was collected. The background and the spectrum of the zeolite with CO were collected. Afterwards, the CO was desorbed and 2 μL of C_9H_{20} were injected (in order to cover all the internal sites). After a few minutes, the excess nonane was desorbed for 20 minutes at room temperature and approximately 7,5 torr of CO were introduced in the system. Spectra were collected for 30 minutes and then CO was evacuated into the room.

The FTIR instrument used is presented in figure 27. It is a *Thermo Scientific Nicolet iS10* spectrometer with a DTGS detector with KBr windows, a KBr beamsplitter and an optical velocity of 0.4747 cm/s. All spectra were collected in transmission mode, with a resolution of 4 cm^{-1} and 64 scans/spectrum, except the CO gas phase spectra, which were collected with a resolution of 1 cm^{-1}. Background spectra were collected before each main spectra collection.

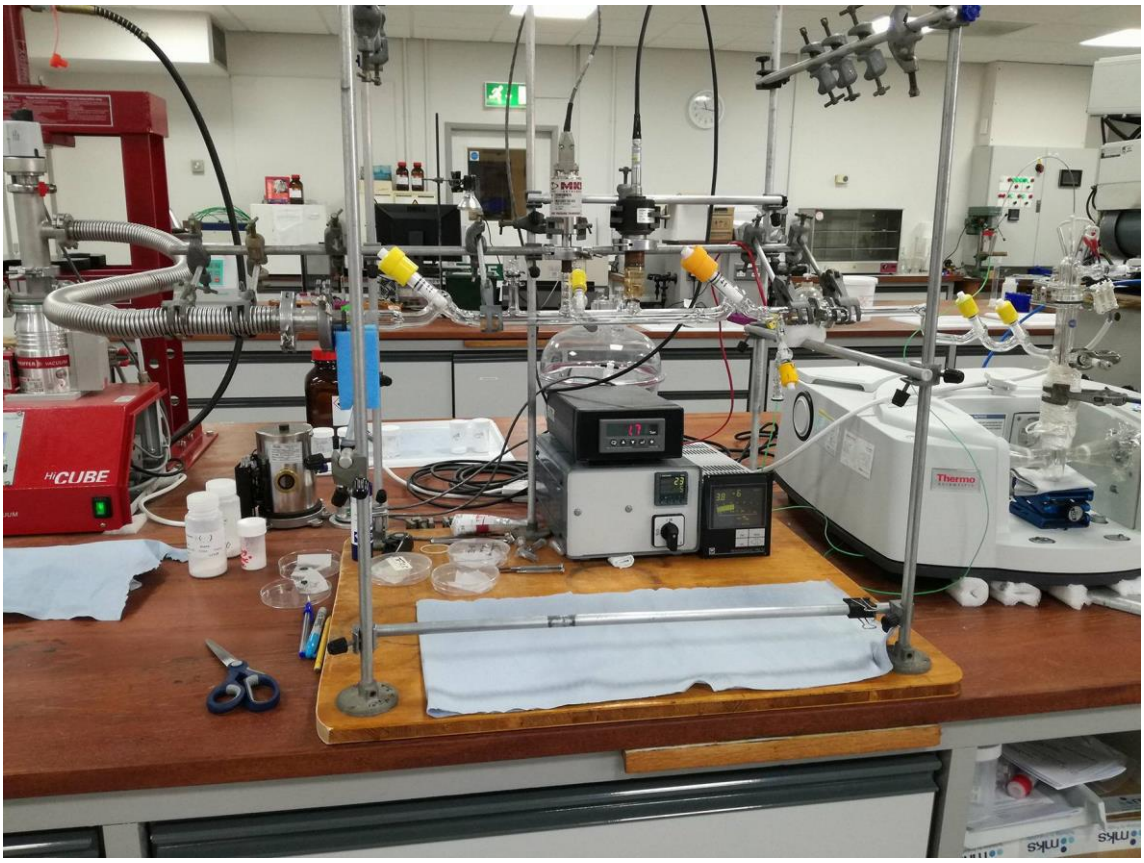

Figure 27 - FTIR experimental setup

3.2.4. Scanning Electron Microscopy (SEM)

Scanning Electron Microscopy is a type of electron microscope that scans the sample's surface with a focused beam of electrons, producing images containing information about its surface topography and composition. [37]

The electron beam is scanned in a raster pattern and the position of the beam is combined with the detected signal to produce an image. The beam can also be focused at a single point for analysis. [37]

The SEM consists of a lens system, an electron gun, an electron collector, visual and recording cathode ray tubes (known as CRTs) and its electronic system. [37]

As the electrons interact with the sample, they produce secondary electrons, backscattered electrons and characteristic x-rays. These signals are collected by one or more detectors to form images which are then displayed on the computer screen. Secondary electrons provide information about the surface morphology while backscatter electrons provide information on the composition as well. [37]

Backscattered electrons provide an extremely useful signal for imaging in SEM. Their response is due to composition, local specimen surface inclination, crystallography and internal magnetic fields. [34] Secondary electrons are mainly produced as a result of interactions between the sample's electrons and incident electrons, which results in the emission of low-energy electrons. [37]

The x-rays are characteristic of the elements present within the sample and can be measured by energy-dispersive x-ray spectroscopy (EDS). When the emitted x-rays enter the detector, it converts the energy of the created electron-ion pairs into a single voltage pulse to be processed for a thorough analysis. Typically, SEM instruments have integrated EDS systems.

In order to prepare the sample for analysis, a small amount of powdered sample is pressed at 2 ton and placed on an aluminium stub, which was previously covered with a small amount of conductive carbon dag. Afterwards, the stub with the sample impregnated in the glue is left on a hot plate for 1 hour to dry. The sample needs to be carbon coated before being ready for analysis. When the sample is ready, the stub is attached to the sample holder on the SEM instrument. The analysis is started after the chamber is evacuated. The SEM used for this analysis was a *Hitachi TM3000* with a *Quantax 70 EDS* incorporated. A scheme of the SEM instrument is presented in figure 28.

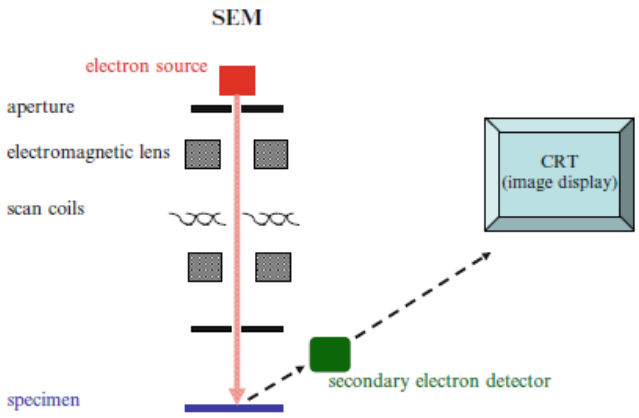

Figure 28 - Scheme of a scanning electron microscope (SEM) [38]

4. Results and Discussion

4.1. Modification Techniques

4.1.1. Ion Exchange

Two solutions of Ammonium Nitrate and Ammonium Acetate 0,1M were prepared in a volume of 200 mL. To prepare the solutions, the calculated amount of ammonium nitrate (or ammonium acetate) and 10 g of zeolite were mixed with 100 mL of water, since the proportion should be 10 mL of H_2O to 1 g of zeolite. This was verified by previous work at Lennard-Jones building at Keele University. The goal of the ion exchange was to limit the amount of Na to 0,5 %. This was not achieved with only one ion exchange, but four.

4.1.2. Mesoporous Surfactant Templated Treatment

As mentioned in chapter 3, four different amounts of citric acid were used to produce the mesopores. By combining the results given by the sorption experiments (where the mesoporosity can be verified) and the results given by the XRD patterns (where the crystallinity can be seen), it was concluded that the optimum amount of citric acid is 4,5 meq. This result will be discussed in more detail on the following subchapters.

4.2. Sorption Analysis

For better understanding of this work, table 4 is presented again, with all samples prepared and their treatments:

Sample name	Sample nr	Description
NH4Y IE	1	Starting material: NaY from Zeolyst Sample was ion exchanged 4 times with NH_4NO_3 and NH_4CH_3COO. Two samples resulted but were treated as only one, since their properties were the same.
NH4Y 6	2	Starting material: NH4Y IE After the ion exchange, sample received mesoporous templated surfactant treatment with 6 meq citric acid

NH4Y 6 calcined	3	Starting material: NH4Y IE After the ion exchange, sample was calcined and then received mesoporous templated surfactant treatment with 6 meq citric acid
NH4Y 4.5	4	Starting material: NH4Y IE After the ion exchange, sample received mesoporous templated surfactant treatment with 4.5 meq citric acid
NaY 6	5	Starting material: NaY from Zeolyst Sample received mesoporous templated surfactant treatment with 6 meq citric acid and then was ion exchanged with NH_4CH_3COO.
NaY 4.5	6	Starting material: NaY from Zeolyst Sample received mesoporous templated surfactant treatment with 4.5 meq citric acid and then was ion exchanged with NH_4CH_3COO.
Original NaY		NaY from Zeolyst
Original NH4Y		NH4Y from CROSFIELD

The N2 sorption experiments are presented below. Figure 29 shows the isotherms obtained for all the samples. As mentioned before, the characteristic shape of an isotherm of a mesoporous material is similar to the type IV isotherms, which have a more pronounced step. To properly compare and analyse the results, each sample is in a separate graph.

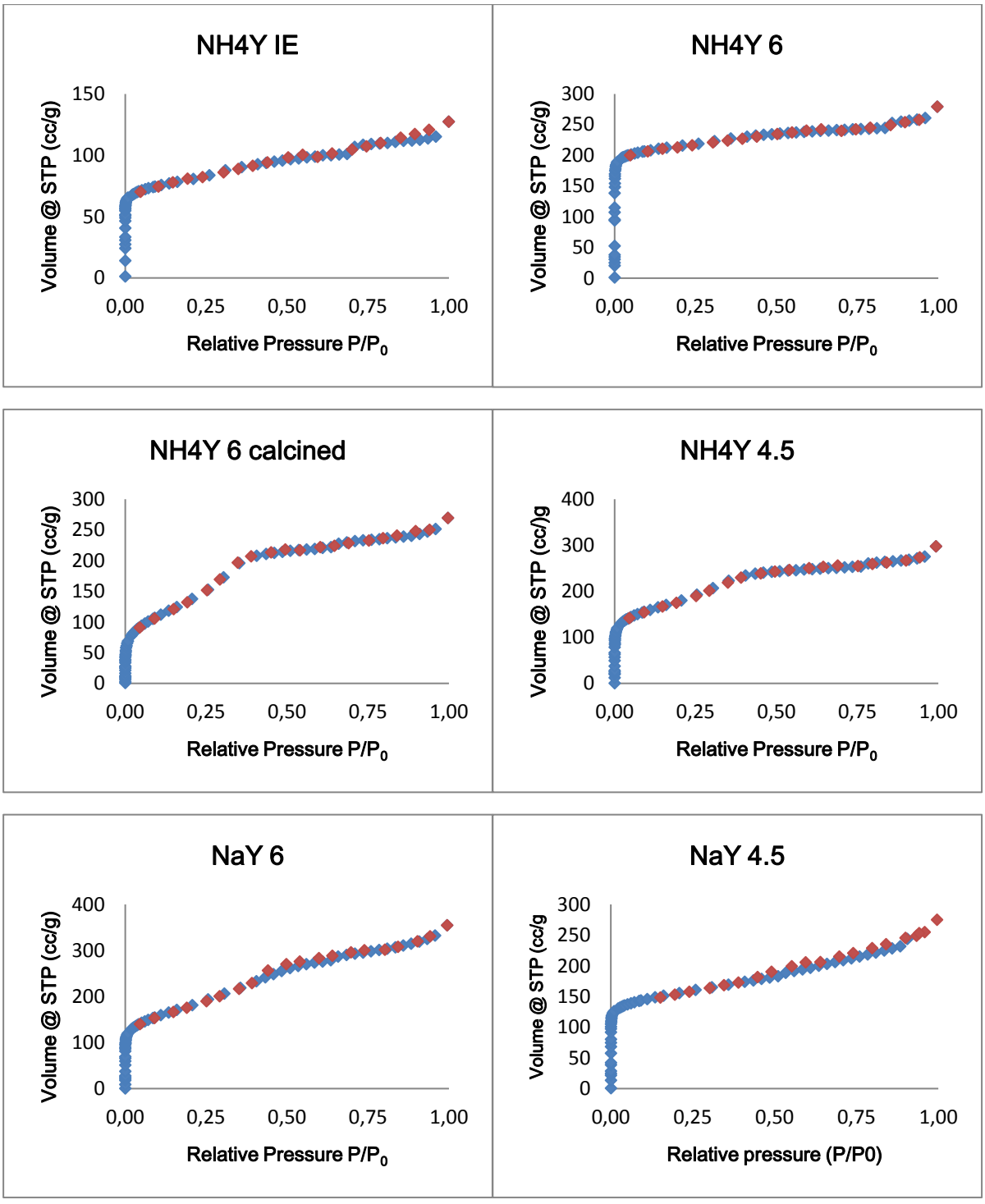

Figure 29 -N2 sorption isotherms for all samples

The isotherms obtained look like a combination of types I, II and IV. Sample 1, which is the sample just ion exchanged to NH_4 form, presents a high inclination for low pressures, due to interactions in micropores leading to the filling of the micropore layer at very low pressures. The rising in the curve is an indicator of monolayer-multilayer adsorption up to high pressures. Sample 2 has a similar

behaviour, however it has a subtle “landing”, possibly approaching a limiting value. This sample was expected to be type IV isotherm, since it was treated with citric acid to create mesopores; the shape of the isotherm is a first indicator that the procedure did not work out the way it should. Samples 3, 4 and 5 have clearly a type IV curve, sample 3 being more noticeable. Sample 6 was expected to be similar to a type IV isotherm as well, although it is very little discernible. Hysteresis was not found in any of the samples.

Surface area was calculated using the t-method (external and internal surface area) and *MultiPoint BET* method. The results are shown on figure 30.

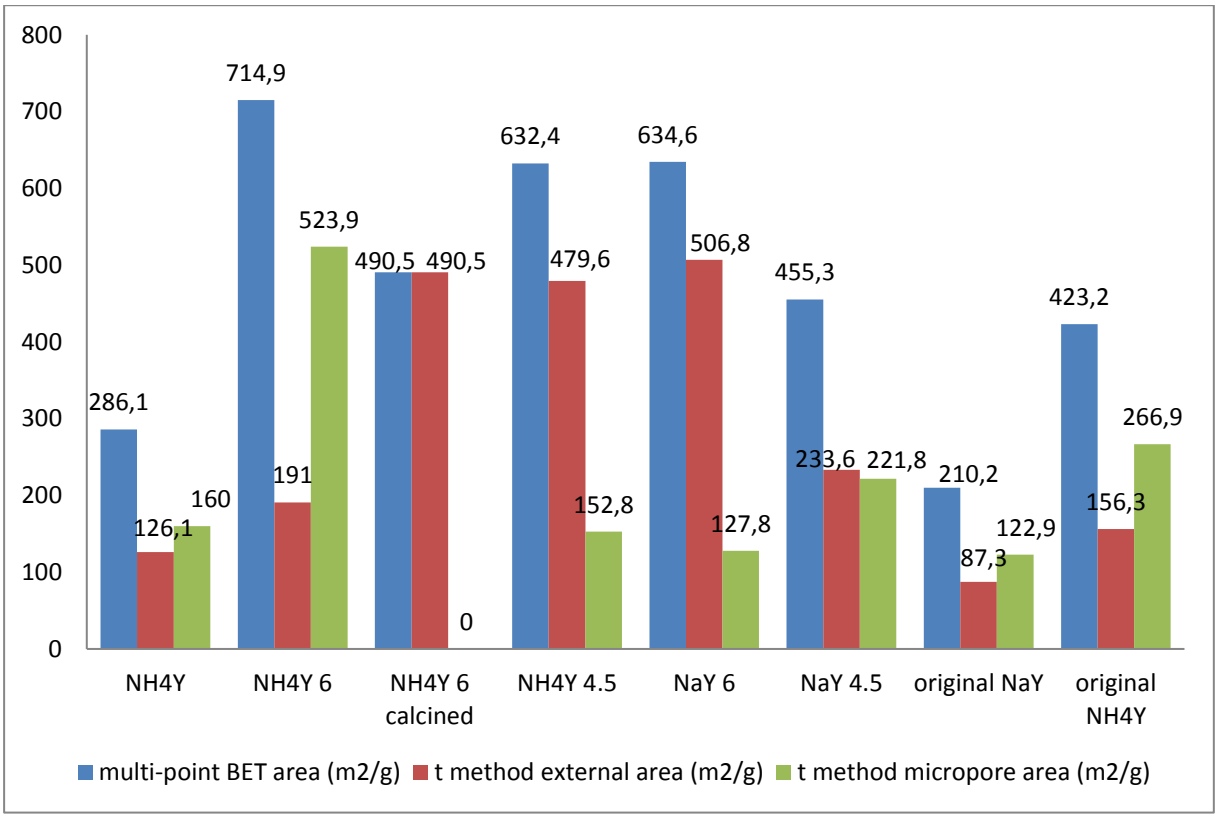

Figure 30 - MultiPoint BET and t-plot methods for all samples

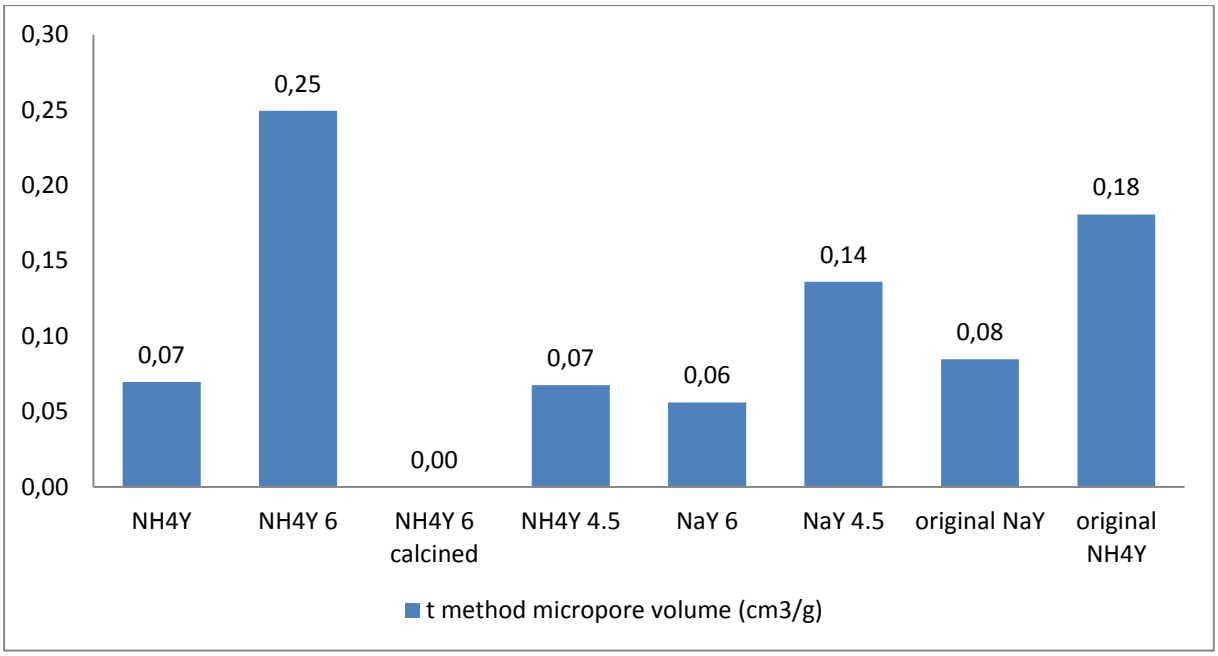

Figure 31 - t-method micropore volume for all samples

Sample 3 (NH4Y 6 calcined) has high surface area, but it was amorphous (as it will be shown further ahead), so it appears to have a surface area bigger than the original sample (original NH4Y), but in fact its crystallinity is very low and no micropores exist. Sample 2 presented an odd result, since it appears to have a larger surface area than the starting material, but in fact its crystallinity is very low so it was considered to be amorphous material. In the original samples and in sample 1 (NH4Y) the total surface area is approximately evenly split between external and micropore surface areas, as expected, since these samples have only micropores. Samples 4 and 5 (NH4Y 4.5 IE and NaY 6 IE) have the biggest difference in external and micropore areas, which indicates that there might have been an increase in the mesoporosity. It should be noted that all this data depends on the instrument and the calculation model used.

The micropore volume was calculated using the t-plot method. Samples 4 and 5 have the lowest micropore volume, indicating the presence of mesopores. Sample 2 presents more micropores than the original NH4Y sample, and that is not possible. This could mean that the equipment used is not 100% reliable, and it is required better equipment to obtain better results. This technique cannot be used quantitatively, only qualitatively.

To determine pore size distribution and diameter, the DFT (density functional theory) was used. The calculation model used by the *Quantachrome ASiQwin 3.0* software was *NLDFT adsorption branch*. The DFT pore size distributions are presented in separate graphics to a better analysis of the results.

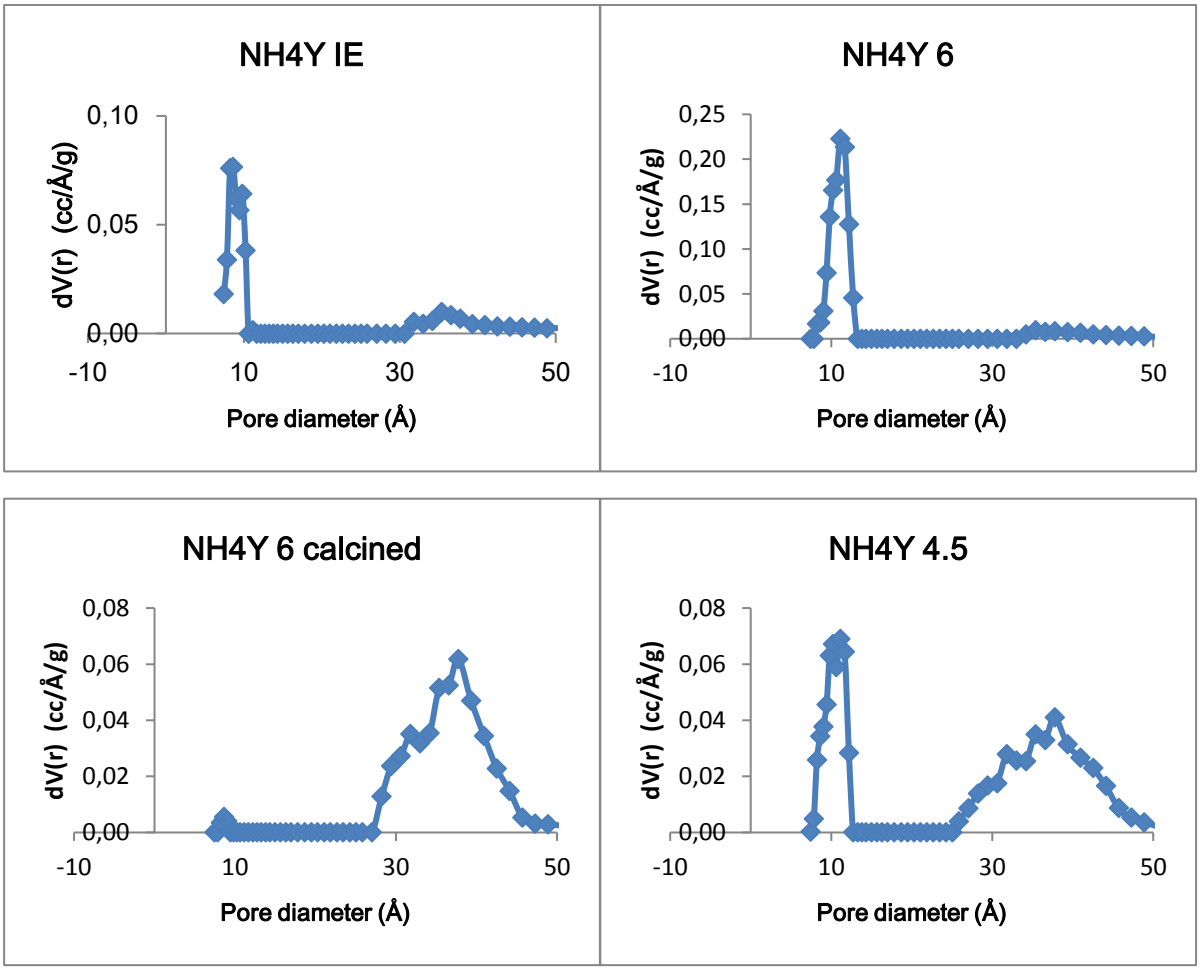

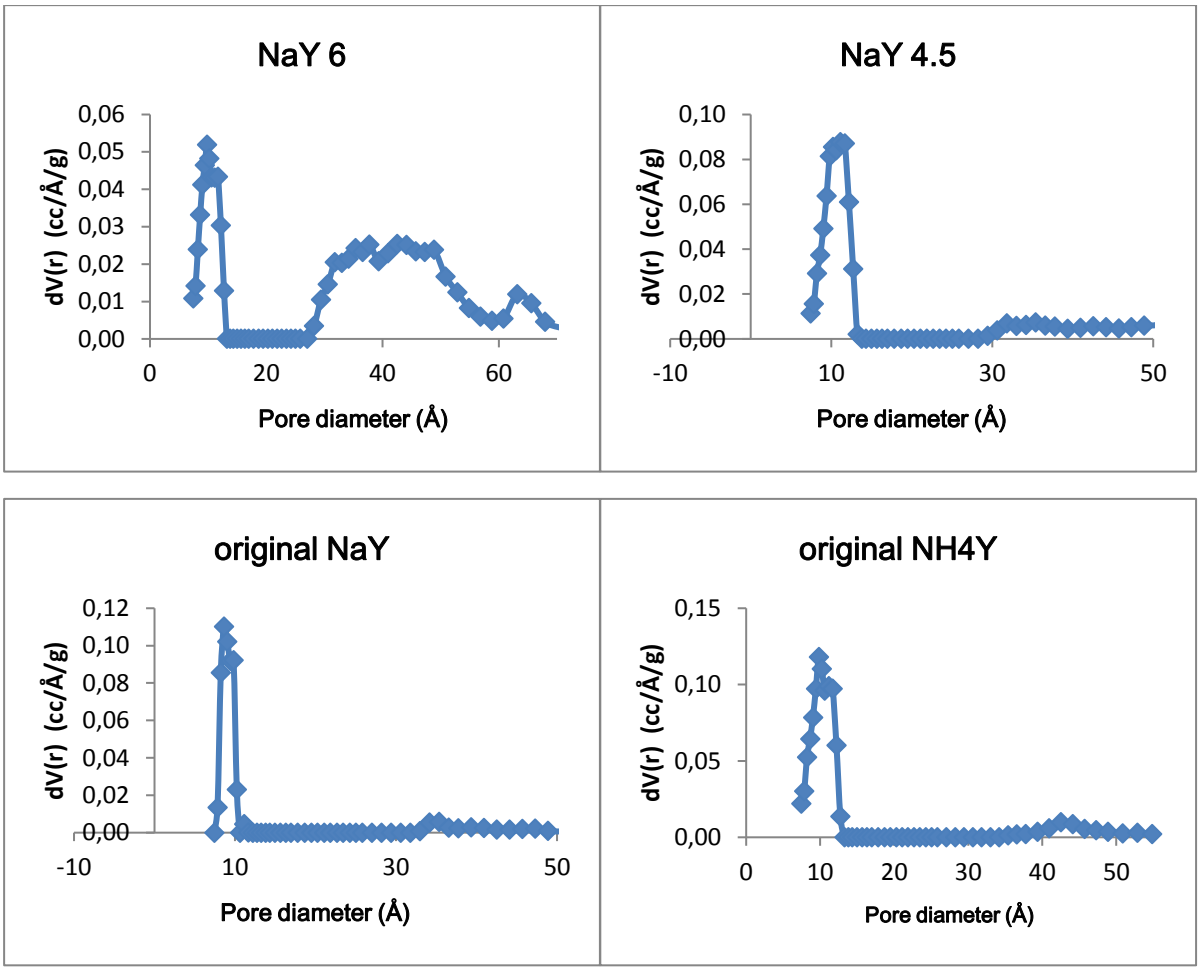

Figure 32 - DFT pore size distribution for all the samples

Mesopores, as mentioned before, correspond to pore sizes between 20 and 500 Å. Samples 1 and 2 clearly have only micropores of about 8 and 10 Å, respectively. It can be seen a small peak around 35 Å in sample 1, which can be due to the instrument used and the liquid nitrogen that moves or pores between particles, and not really mesopores. Sample 3 can be misleading, since it appears to have mesopores ate about 40 Å but it is amorphous material (as this sample was destroyed). Samples 4 and 5 both have mesopores of about 40 Å, as expected. Sample 6 was also expected to have mesopores; however, it only presents a very small amount of mesopores around 30 Å.

The pore diameter can be found in Figure 33:

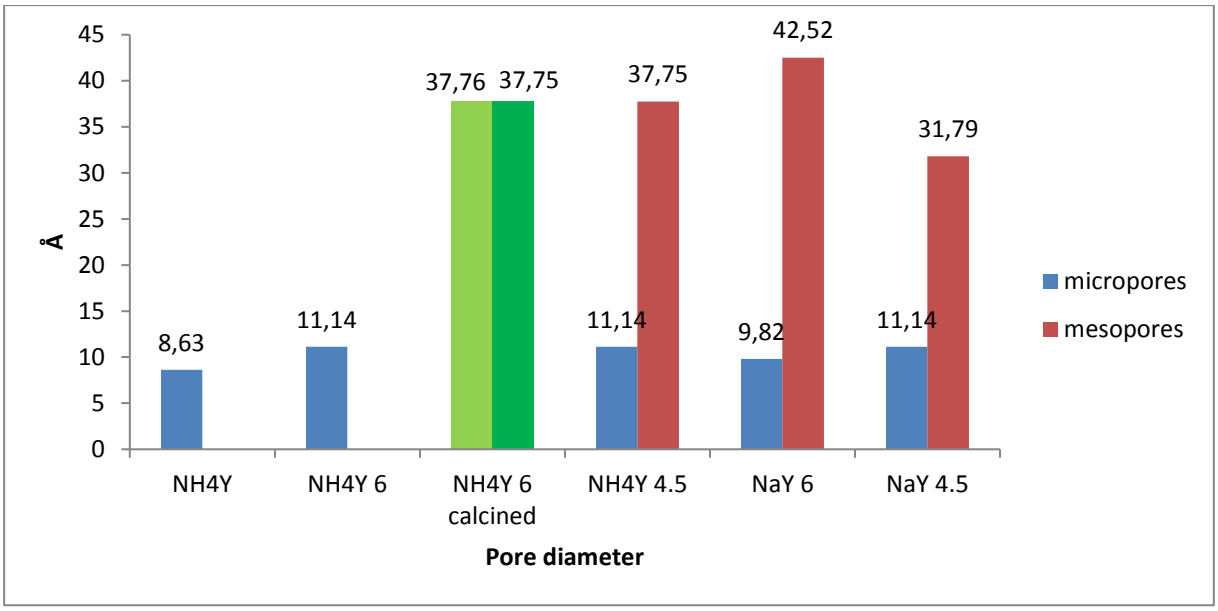

Figure 33 - DTF pore diameter of micro and mesopores for all samples

Sample 3 (NH4Y 6 calcined) is in a different colour due to its loss of crystallinity. It is amorphous, so it does not have micropores nor mesopores. A summary of all the data obtained in the sorption experiments can be found in Tables A1 and A2, Appendix A.

Considering the sorption data results individually, it is not possible to decide which route is better (route 1 or 2), since the two samples with more mesopores are sample 4 and sample 5 and they were prepared by different routes and using different amounts of citric acid. Thus, conclusions cannot be drawn from this characterization technique alone, they need to be combined with the results from all techniques. Also, the results obtained are not the best. This is due, amongst other factors, to the fact that the activation and the analysis are not in the same place (the sample holder is moved to another station) and Argon being a better sorption gas than the one used in the experiments (N_2) because it allows the pore size distribution to be obtained as a continuous curve for a wide range of pore sizes.

4.3. X-ray diffraction (XRD)

X-ray diffraction patterns were used to study the crystallinity of the samples, in order to understand which treatments provoke a smaller loss of crystallinity. Unit cell size was also calculated using silicon as an X-ray internal standard. The XRD patterns obtained are presented in Appendix B.

The relative crystallinity was calculated according to *Standard Test Method for Determination of Relative X-ray diffraction Intensities*. [39] The main equation used was the following:

$$\%XRD = \frac{S_X}{S_R} \times 100 \quad (4)$$

where S_X is the sum of integral peak intensities for the sample and S_R the sum of the integral peak intensities for the reference "original NH4Y".

In table 6 are the relative crystallinity percentages for all samples, using the original NH4Y from CROSFIELD as 100%.

Table 6 - % crystallinity of all samples

Sample name	Sample nr	%XRD	%XRD with silicon standard
NH4Y IE	1	98,1%	100,4%
NH4Y 6	2	56,6%	35,2%
NH4Y 6 calcined	3	0,19	0,1%
NH4Y 4.5	4	19,9%	18,8%
NaY 6	5	50,8%	49,8%
NaY 4.5	6	71,8%	70,95%
Original NaY		94,3%	100%
Original NH4Y		100%	100%

Samples 2 and 4 are inconsistent: sample 2 was expected to be more crystalline, since it suffered a treatment less severe than sample 4. However, from previous BET analysis, it was suspected

that the treatment in sample 2 did not work properly, not forming mesopores, hence the superior crystallinity. Due to this unexpected result, all the crystallinity percentages were repeated using the XRD patterns with the silicon standard.

Using an internal standard is a more efficient way to ensure the results are accurate, since they all have the same "baseline". After comparing both crystallinity results it was decided to use the results obtained with the internal standard in all further calculations and reasoning.

Sample 3 is obviously destroyed, since its crystallinity is nearly 0. Comparing the two different routes in study, route 2 is more effective. Na^+ is more stable than $NH4^+$, and that reflects on the crystallinity results: the two samples on route 2 are more crystalline than the samples on route 1. Between those two (sample 5 and 6), sample 5 appears to have more mesopores, but since its crystallinity is around 50%, some of that may be amorphous material. Hence, sample 6 can be considered the best sample, since it had little crystallinity loss and a reasonable amount of mesopores. Ergo, the optimum amount of citric acid is concluded to be 4,5 meq.

Unit cell size was calculated according to [31] and [39]. The diffraction angle calculated for Si is 56,123º. The d-spacing (d_{hkl}) and the unit cell dimension (a) were calculated, and the measured values of the angles were corrected using a correction factor based on the calculated value for silicon that was added to the measured values of the zeolite reflections.

$$d = \frac{\lambda}{2sin\theta} \quad (5)$$

$$a = \{(dhkl)^2\ (h^2 + k^2 + l^2)\}^{1/2} \quad (6)$$

$$correction\ factor = 2\Theta\ (calculated\ for\ Si) - 2\Theta\ (measured\ for\ Si) \quad (7)$$

With the unit cell dimension (a) it was possible to calculate the Si/Al ratio in the framework, using the average value (a_0).

$$N_{Al} = 115.2(a_0 - 24.191) \quad (8)$$

$$\left({}^{Si}/_{Al}\right) = \frac{192 - N_{Al}}{N_{Al}} \quad (9)$$

With 25,191 being the unit cell dimension of a Faujasite zeolite with $N_{Al} = 0$. The results are presented in table:

Table 7 - XRD unit cell size results

	hkl 243 measured	hkl 243 corrected	hkl Si measured	hkl Si corrected	hkl 211 measured	hkl 211 corrected	correction factor
NH4Y IE	58,178	58,189	56,112	56,123	53,870	53,881	0,011
NH4Y 6	58,598	58,644	56,077	56,123	54,208	54,254	0,046
NH4Y 6 calcined	amorphous						
NH4Y 4.5	58,697	58,678	56,142	56,123	54,317	54,298	-0,019
NaY 6	58,447	58,468	56,102	56,123	54,139	54,160	0,021
NaY 4.5	58,414	58,436	56,101	56,123	54,072	54,094	0,022
original NaY	58,254	58,273	56,104	56,123	53,947	53,966	0,019
original NH4Y	58,168	58,178	56,113	56,123	53,865	53,875	0,010
	d243	**d 211**	**a 243**	**a 211**	**a average**	**N_{Al}**	**Si/Al**
NH4Y IE	1,584	1,700	24,695	24,697	24,696	58,142	2,302
NH4Y 6	1,573	1,689	24,520	24,540	24,530	39,029	3,919
NH4Y 6 calcined	amorphous						
NH4Y 4.5	1,572	1,688	24,507	24,521	24,514	37,225	4,158
NaY 6	1,577	1,692	24,587	24,579	24,583	45,171	3,251
NaY 4.5	1,578	1,694	24,599	24,607	24,603	47,475	3,044
original NaY	1,582	1,698	24,662	24,661	24,661	54,198	2,543
original NH4Y	1,584	1,700	24,699	24,699	24,699	58,534	2,280

As expected, the samples that suffered the surfactant-templated mesoporous treatment have smaller unit cell size than the original zeolites. Increasing mesoporosity causes decreasing the unit cell size due to a slight dealumination by the citric acid. However, the sample with the smallest unit cell is sample 4 and the BET results suggest that the sample with more mesopores is sample 5. Looking at table 7 it can be concluded that route 1 is better, since the two samples with smaller unit cell size are 2 and 4, but knowing the % crystallinity of the samples the conclusion if different. Samples 2 and 4 have

less crystallinity, so some of the mesoporosity can be amorphous material. Hence, Route 2 appears to be more effective.

Comparing the $(Si/Al)_{framework}$ with the global Si/Al ratio given by the SEM experiments, the first one should be bigger, since creating mesopores is removing Al atoms from the framework. These two ratios will be compared in the next chapter.

4.4. SEM/EDS

SEM images give information on the shape and size of the particles, whereas EDS measurements have information on the elemental composition of the zeolite samples.

The SEM images were collected in the Lennard-Jones laboratory, with the exception of samples 1 and 3, which were taken to the SEM instrument in Manchester University, since the quality of the images obtained there is much higher. Sample 6 does not have a representative image of its particles, there was a problem with the SEM instrument. All results are presented in Figure 34, with different magnifications.

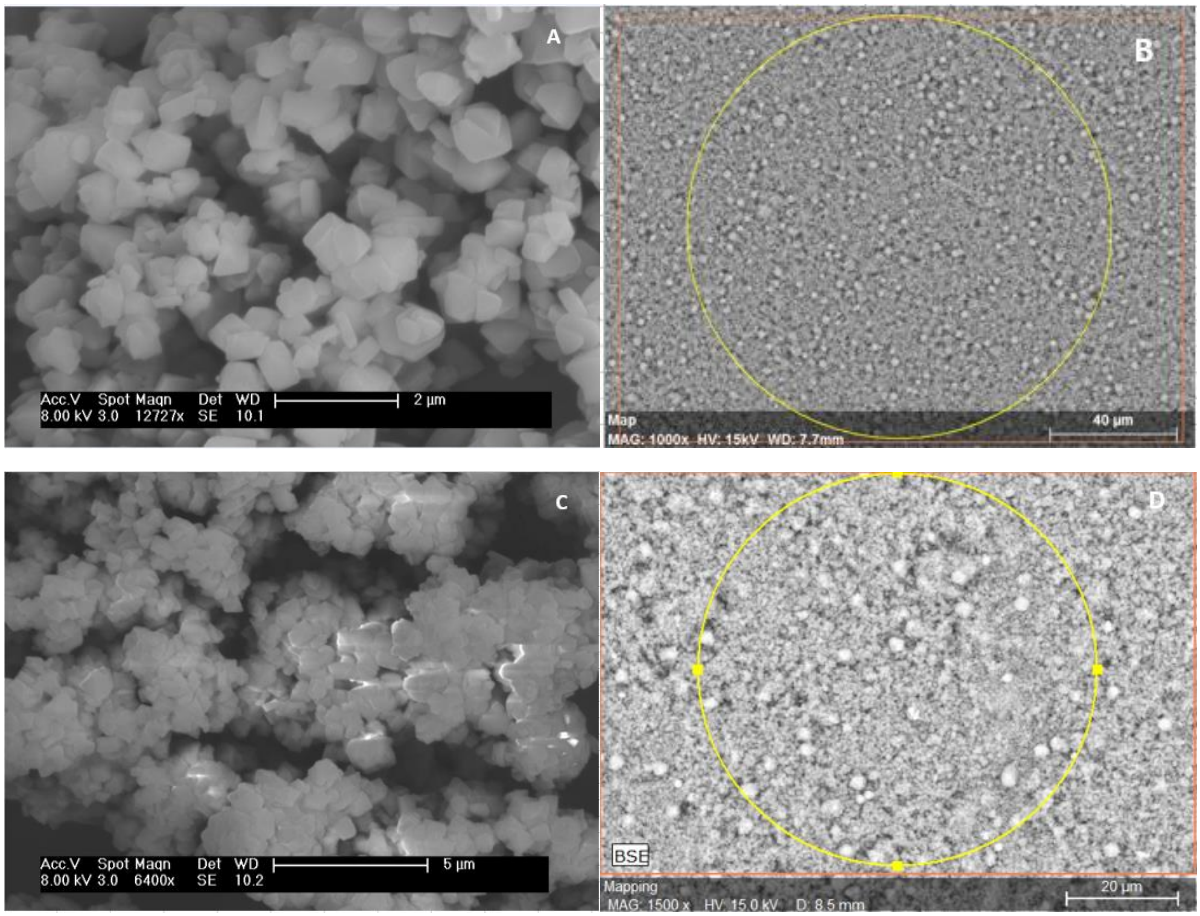

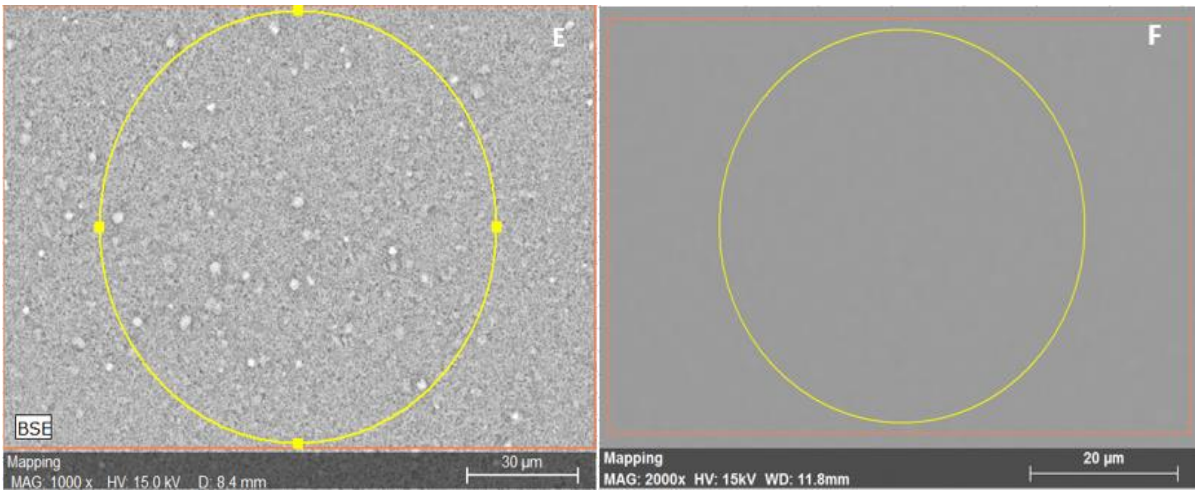

Figure 34 - SEM images: Sample 1 (A), Sample 2 (B), Sample 3 (C), Sample 4 (D), Sample 5 (E), Sample 6 (F)

In the first 4 samples, the particles appear to be evenly distributed. Sample 3 can be misleading, since it seems to have crystals, but it is known from XRD results that the samples is amorphous. Sample 5 appears to have some particles bigger than others, however homogeneous in shape. No conclusions could be drawn from image F regarding sample 6. It should be noted that, the higher the magnification, the lower the quality of the images.

After the SEM, EDS measurements were made. From them it was possible to estimate the Si/Al ratio and the %Na in the samples. The spectra obtained in EDS experiments can be seen in Figures C1 to C6 Appendix C, and the following table summarizes the data achieved from there.

Table 8 – Composition of all samples

	Si/Al	Na/Al	%Na
NH4Y IE	2,5	0,168	1,47%
NH4Y 6	2,77		
NH4Y 6 calcined	7,79	0,095	0,22%
NH4Y 4.5	4,03	0,244	1,48%
NaY 6	3,84	0,210	0,76%
NaY 4.5	3,39	0,184	0,73%
original NaY	2,51	0,989	7,82%
original NH4Y	2,37	0,204	0,88%

Sample 1 has a Si/Al very similar to the original samples, as expected. In sample 2, the sodium atom was not detected. The Si/Al obtained in sample 2 is another indication that the mesoporous treatment did not work as expected, since the Si/Al ratio is approximately the same as the original samples. In addition to that, the BET results also lead to that conclusion. Sample 3, as it is destroyed, presents the higher Si/Al ratio, which is already known that is due to the loss of crystallinity. In mesoporous samples, the Si/Al ratio is expected to increase to about 3-5. [21] This is the case of samples 4, 5 and 6.

Regarding the sodium percentages, original NaY has naturally a much higher percentage than all other samples. Sample 4 has a sodium percentage far too high, since it is bigger than the original NH4Y sample, which is not possible. Samples 5 and 6, as expected, have a slightly higher %Na, since they were made by route 2: Na^+ is more stable than NH_4^+, and being ion exchanged in the end of the route it has more residual Na atoms than the samples made by route 1. Moreover, there was always a residual amount of sodium in all samples: it is very difficult to remove it completely because it gets trapped in the sodalite small cages.

Table 9 presents the Si/Al ratios obtained by SEM/EDS and the $(Si/Al)_{framework}$ obtained by XRD experiments:

Table 9 - Si/Al global and framework ratios for all samples

	Si/Al (SEM)	Si/Al framework (XRD)
NH4Y IE	2,5	2,30
NH4Y 6	2,77	3,92
NH4Y 6 calcined	7,79	-
NH4Y 4.5	4	4,16
NaY 6	3,84	3,25
NaY 4.5	3,39	3,04
original NaY	2,51	2,54
original NH4Y	2,37	2,28

In theory, the $(Si/Al)_{framework}$ should be higher than the global Si/Al ratio, considering that some of the aluminium atoms are outside the framework. In the samples prepared by route 1 (samples 2 and 4) this result is verified. Yet, in samples 5 and 6 (route 2) the $(Si/Al)_{framework}$ is lower than the global Si/Al ratio. This can indicate a slight desilication by the acid treatment, existing some extra-framework Si in the form of amorphous silica.

4.5. Infrared Spectroscopy

The IR analysis was divided into two parts: pyridine adsorption to quantify the acid sites in zeolite Y and using various probe molecules to distinguish between external and internal pores.

4.5.1. Pyridine Adsorption

The collected spectra are presented below. All spectra were analysed in the 4000–1400 cm-1 region, and they were all scaled to 10 mg/cm^2 to do proper comparisons. All spectra were collected before the pyridine injection (after activation at 450ºC) and after pyridine desorption at 150, 200, 250, 300, 350, 400 and 450ºC. Two major zones were analysed: pyridine (Brønsted and Lewis corresponding peaks - the vibration of molecules adsorbed on Brønsted sites in the form of pyridinium ions and pyridine coordinatively adsorbed on Lewis acid sites), the silanols and the bridging OH groups (low frequency – LF- and high frequency –HF- OH groups). The spectra before pyridine injection was subtracted to each desorption spectra, to obtain only the acid sites that interact with pyridine. The subtraction results for all samples can be found in figures D1 to D6 in appendix D.

Figure 35 shows the pyridine desorption spectra at 200ºC, zoomed in the pyridine region (1700-1400 cm^{-1}):

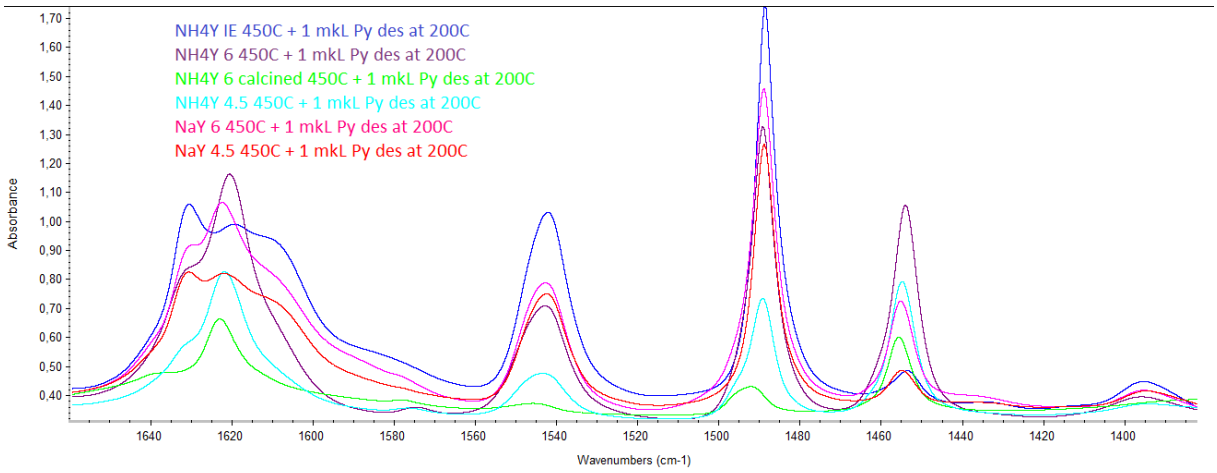

Figure 35 - IR spectra of pyridine desorption at 200C in all samples

Brønsted acid sites appear around 1540 cm^{-1} and Lewis acid sites around 1450 cm^{-1}. Sample 2 (NH4Y 6) presents much more LAS than any other sample. Sample 3 (NH4Y 6 calcined) is destroyed,

it has some LAS but very few BAS. The samples created by route 2 present more BAS than the ones prepared by route 1.

Figure 36 shows the spectra of all samples before pyridine injection, zoomed in the OH region (3800-3450 cm^{-1}).

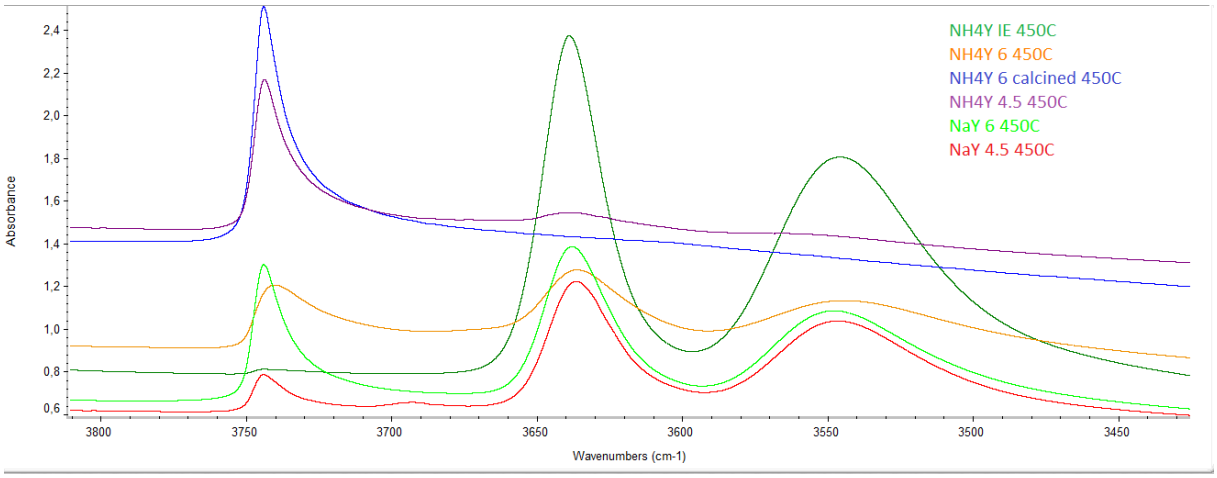

Figure 36 - IR spectra of all samples before pyridine injection

The OH groups divide in three categories: silanols, LF bridging OH groups and HF bridging OH groups. Low frequency OH groups appear around 3545 cm^{-1}, high frequency groups appear around 3630 cm^{-1} and silanols at about 3745 cm^{-1}.

When a zeolite structure is destroyed, OH groups are removed first, followed by Al-O bonds, and then they begin to lose micropores and crystallinity. Samples 3 (NH4Y 6 calcined) and sample 4 (NH4Y 4,5) do not have bridging OH groups, as expected, since sample 3 is destroyed completely and sample 4 has very low crystallinity (about 20%). The intensity of all OH groups in samples prepared by route 2 is higher than the samples made by route 1, another indicator that route 2 is more effective.

Figure 37 shows the two previous graphics subtracted, both zoomed in the OH region, in order to analyse the accessibility of OH groups.

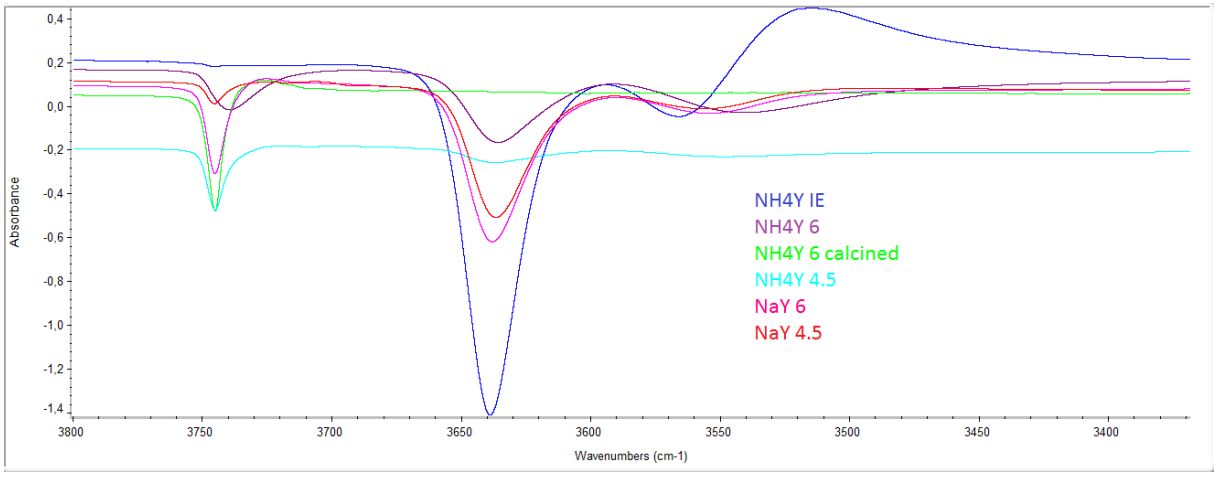

Figure 37 - IR spectra of pyridine desorption at 200C subtracted by spectra before pyridine injection for all samples

Low frequency OH groups are almost not accessible to pyridine, as seen in figure 37. High frequency OH groups and silanols are all accessible. Analysing figure 37, it can be seen that LF's in the samples prepared by route 2 are more accessible than in samples prepared by route 1. Silanols appear to be very accessible in samples 3 and 4, but that is due to their loss of crystallinity.

Based on the peak heights of the spectra of pyridine desorption at different temperatures, the amount of Lewis and Brønsted acid sites in the samples was calculated.

Table 10 - Amount of Brønsted and Lewis acid sites in all samples

	Py-BAS (mmol/g)	Py-LAS (mmol/g)
Sample 1	1,054	0,142
Sample 2	0,664	1,156
Sample 3	0,068	0,407
Sample 4	0,228	0,748
Sample 5	0,796	0,623
Sample 6	0,656	0,177
Original NaY	0,002	2,540

The evolution of LAS, BAS and OH groups in all samples is presented in figure 38:

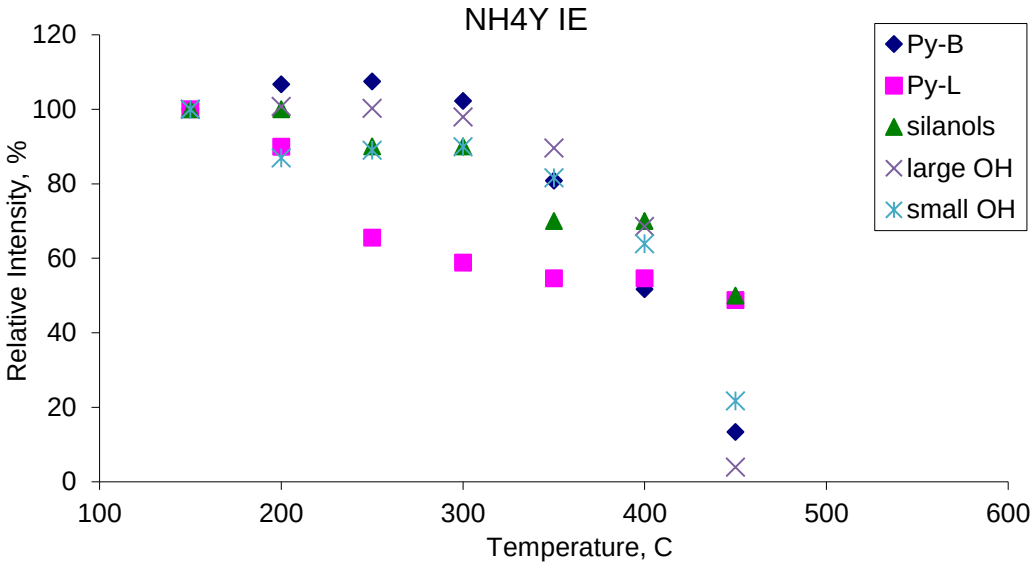
NH4Y IE
Relative Intensity, %
Temperature, C
Py-B
Py-L
silanols
large OH
small OH

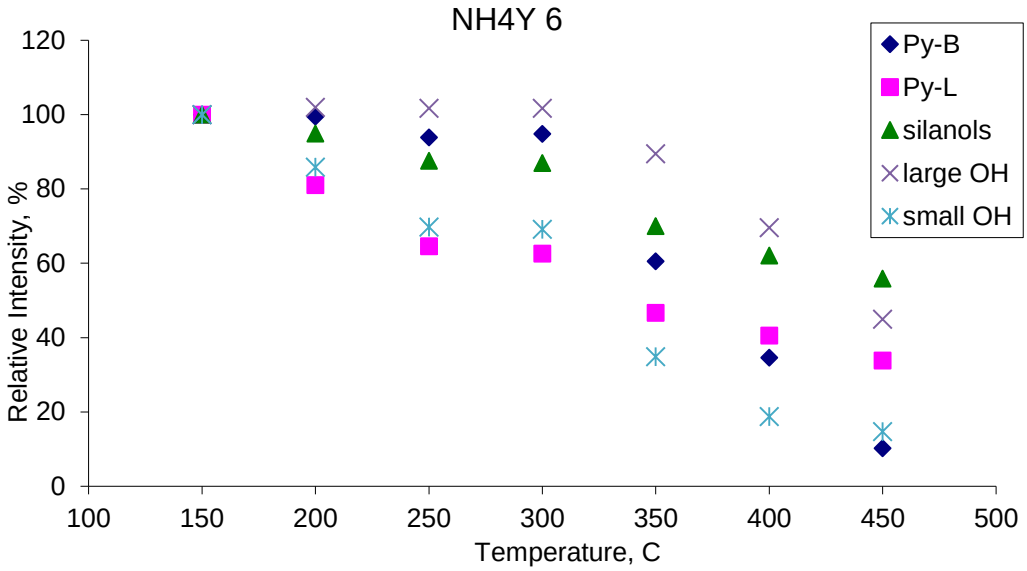
NH4Y 6
Relative Intensity, %
Temperature, C
Py-B
Py-L
silanols
large OH
small OH

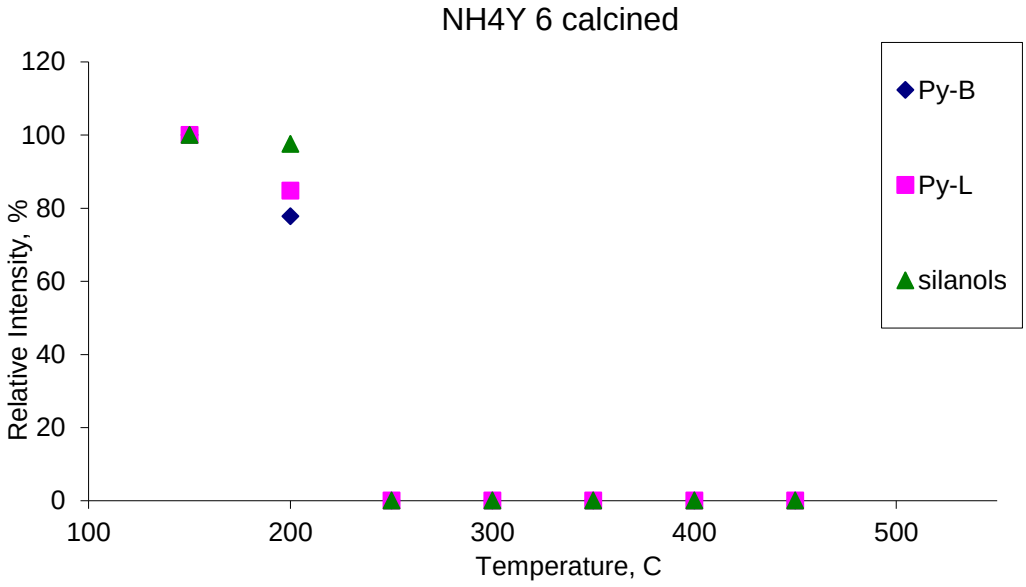
NH4Y 6 calcined
Relative Intensity, %
Temperature, C
Py-B
Py-L
silanols

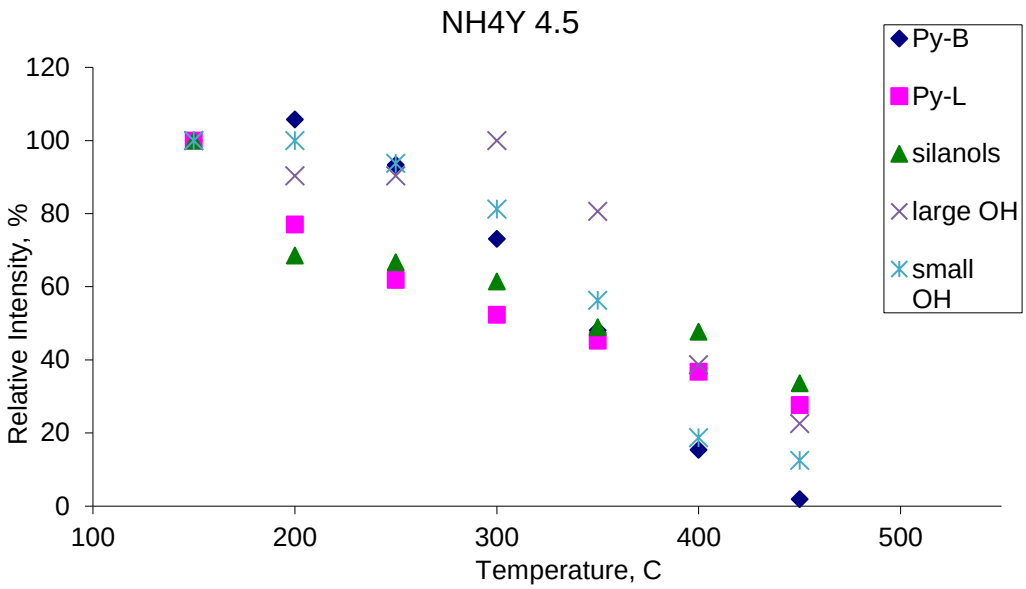
NH4Y 4.5
Py-B
Py-L
silanols
large OH
small OH
Relative Intensity, %
Temperature, C
0
20
40
60
80
100
120
100
200
300
400
500

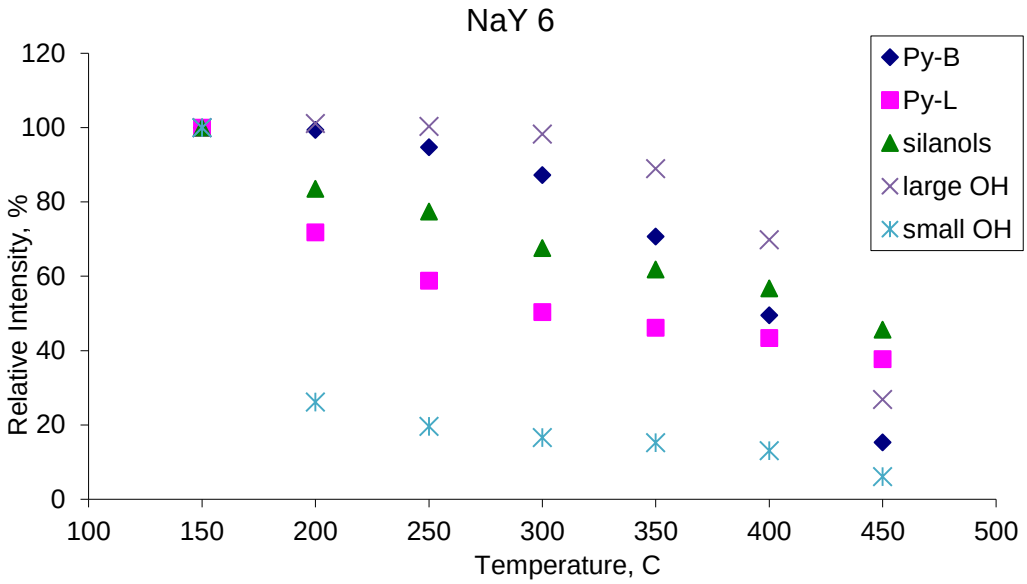
NaY 6
Py-B
Py-L
silanols
large OH
small OH
Relative Intensity, %
Temperature, C
0
20
40
60
80
100
120
100
150
200
250
300
350
400
450
500

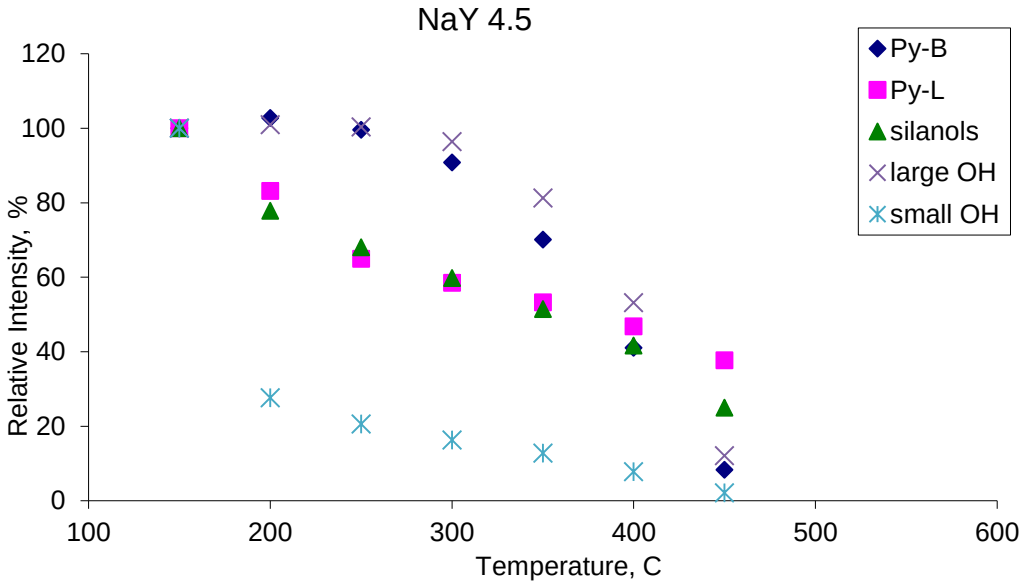
NaY 4.5
Py-B
Py-L
silanols
large OH
small OH
Relative Intensity, %
Temperature, C
0
20
40
60
80
100
120
100
200
300
400
500
600

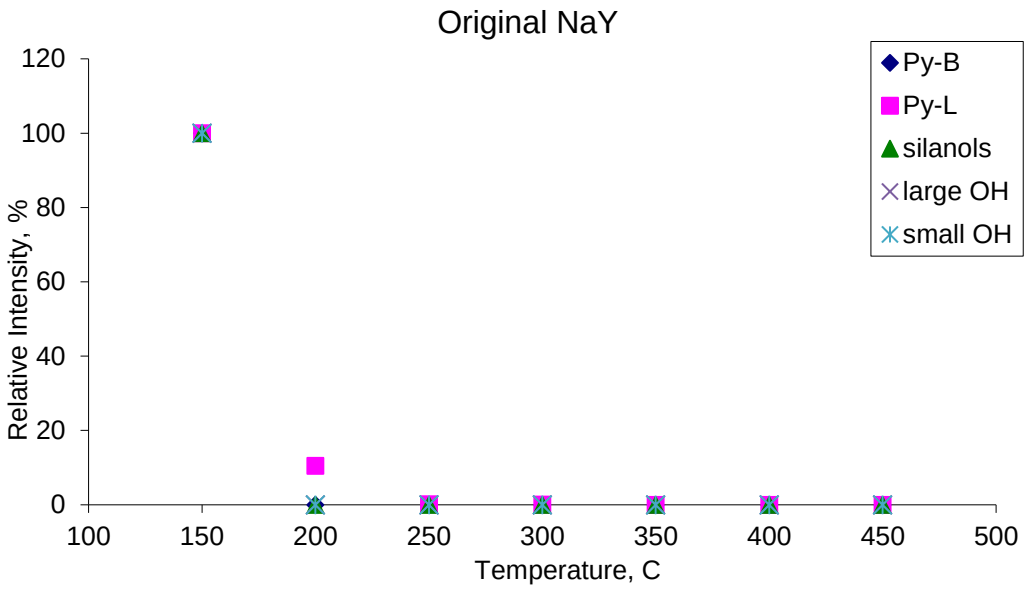

Figure 38 - Pyridine desorption data for all samples

The samples that suffered mesoporous treatment have less Brønsted acid sites and more Lewis acid sites than sample 1 (NH4Y just ion exchanged). On the other hand, the original NaY sample has practically no BAS and a much higher quantity of LAS.

The evolution of the LAS, BAS and OH groups is as expected in all samples. In sample 4, the trend appears to be different, but the experimental data from the 200 ºC should be disregarded and attributed to instrument error. In the samples created by route 2, the amount of OH groups in small cages decreases much faster than in the samples from route 1, as expected, since they have a larger quantity of Na and the original NaY samples has no OH groups (either silanols or bridging OH groups) as from 200 ºC.

4.5.2. Accessibility by different probe molecules

To test the accessibility, several probe molecules were used, as mentioned in previous chapters. The aim was to quantify the external acid sites and so distinguish between micro and mesopores. It should be noted that bridging OH groups are located in the zeolite pores, while silanol groups are located in the external surface. [36] The goal was to block the internal sites with the first molecule, and then adsorption of a different probe molecule. The probe molecules were first injected

individually, to see which ones were worth combining with other. Table 11 summarizes which probe molecule was used in which sample:

Table 11 - Different probe molecules used with each sample

Sample	1st probe molecule	2nd probe molecule
NH4Y IE	C_9H_{20}	CD_3CN
	di-t-Bu-Py	-
	C_9H_{20}	-
	CD_3CN	-
	tri-isopropylbenzene	-
original NH4Y	tri-isopropylbenzene	-
BEA 12.5	C_9H_{20}	CO
ZSM-5 (40)	C_9H_{20}	
ZSM-5 (AK0654)	C_9H_{20}	CO
ZSM-5 (AK0658)	C_9H_{20}	CO

Besides the zeolite in study (zeolite Y), zeolites Beta (BEA) and ZSM-5 (MFI) were also used with some of the probe molecules for comparison, since their behaviour was known from work made by colleagues at the Birchall Centre.

In the di-t-Bu-Py experience, only BAS can be determined, since it is a proton acceptor, so the H^+ proton in Brønsted sites to can interact with the nitrogen atom. Comparing its spectra with the Pyridine spectra, it is possible do distinguish between micro and mesopores. Since di-t-Bu-Py is bigger (7 Å) than pyridine (5,3 Å) [6] [36], only acid sites in the external surface are accessible. However, since the pore size in zeolite Y is about 7,5 Å, di-t-Bu-Py was able to enter the micropores and no distinction could be made (figure 39).

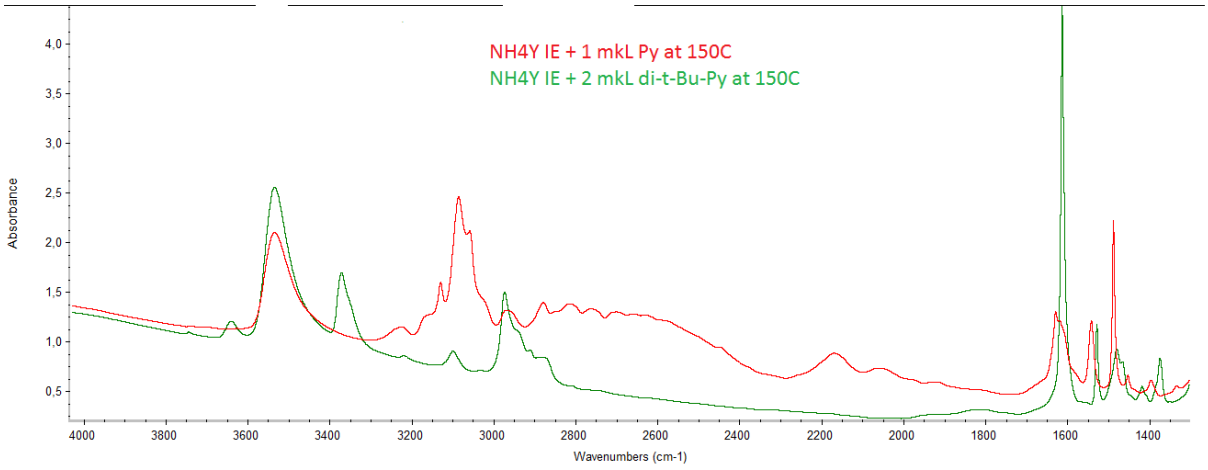

Figure 39 - IR spectra of Py and di-t-Bu-Py injection for sample 1

Afterwards, the experience was made with tri-isopropylbenzene. It's kinetic diameter is 9,3 Å [41], so it should not enter the zeolite pores. Comparing its spectra with pyridine one, it is possible to distinguish between external and internal pores. The results showed a peak around 1450 cm^{-1}, which means that some LAS are in the external surface (in the form of extraframework Al). It did not interact with any silanol groups, though (figure 40).

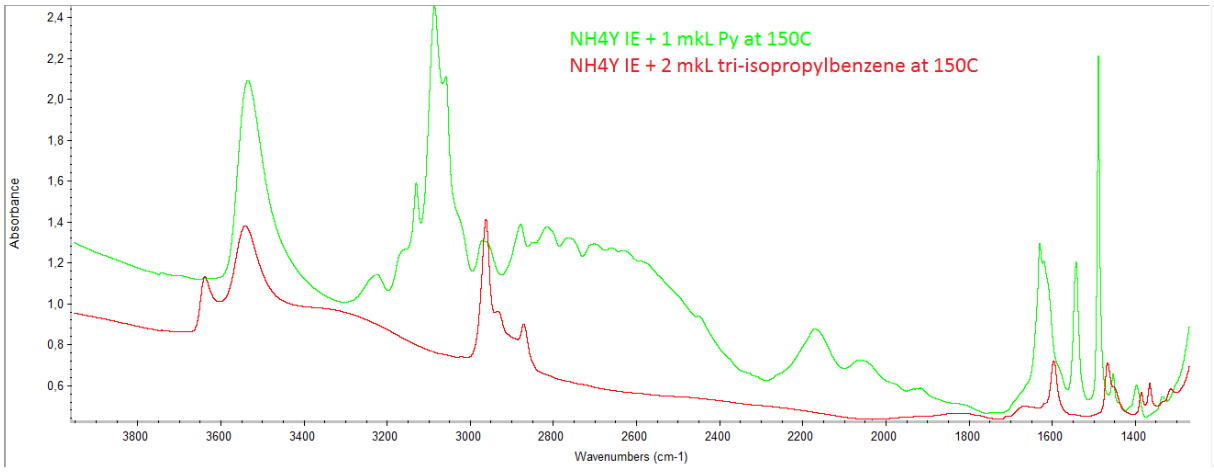

Figure 40 - IR spectra of Py and tri-isopropylbenzene injection for sample 1

The following experience was with deuterated acetonitrile (CD_3CN). Acetonitrile was used deuterated because it is more appropriate for these studies than CH_3CN, as the CH_3CN CN spectral region is strongly complicated by Fermi resonance. [42] Since it is a small molecule (4 Å), it has access to all of the OH groups.[42] [43] It was concluded that CD_3CN interacted with all the OH groups, and that desorption at 100 ºC removes all acetonitrile (figure 41).

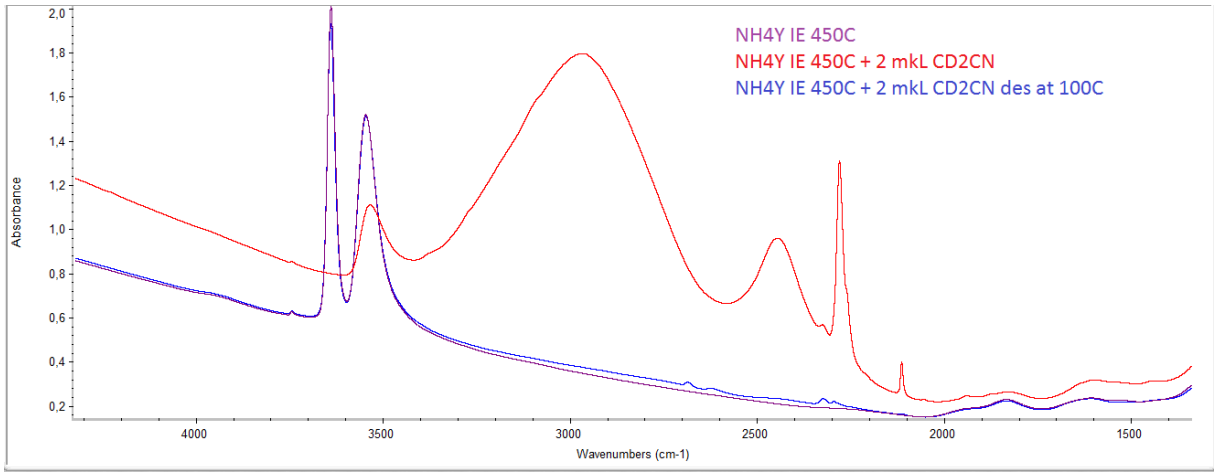

Figure 41 - IR spectra of CD_3CN: before and after injection, and desorption at 100 ºC for sample 1 (NH4Y IE)

It was experimented with nonane as the first probe molecule and acetonitrile as the second, but it was displacing the existing nonane and entering the pores. This spectra can be found in figure D7 appendix D.

Nonane, whose kinetic diameter is 4,3 Å [44] [45], was also tested in sample 1. It clearly interacts with the OH groups in large cages and with LAS, and has a small interaction with silanols. It was the chosen molecule to be the first probe molecule in the following experiences (figure 42).

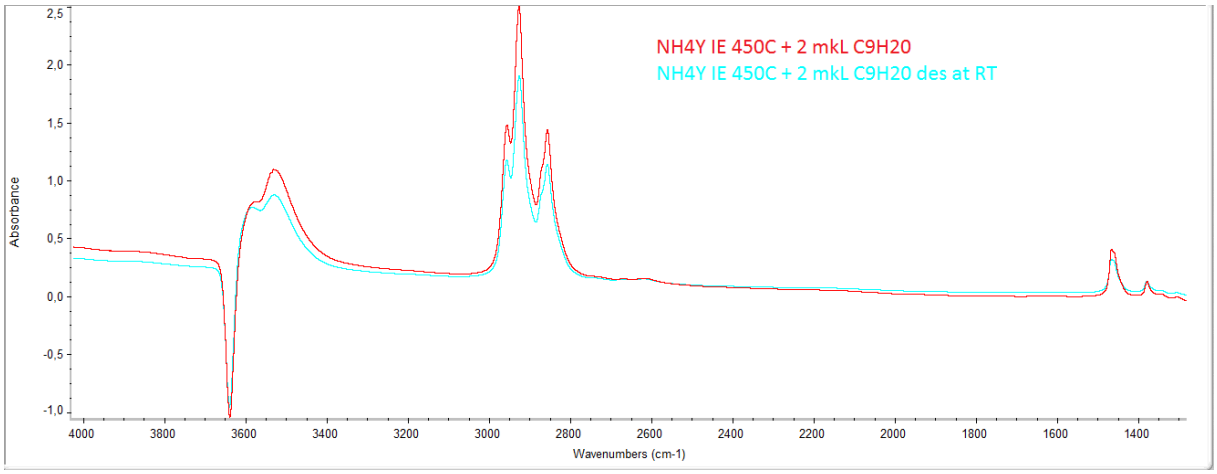

Figure 42 - IR spectra of nonane subtracted by spectra before injection for sample 1 (NH4Y IE)

The second probe molecule chosen was CO. Although it is a small molecule (3,7 Å) [35], it cannot interact with the OH groups in sodalite cages because it cannot physically come into contact with them, when adsorbed at low temperatures. Nonetheless, larger and stronger bases like pyridine or

acetonitrile can interact with those hydroxyls. Being strong bases, they attract the protons forcing them out of the sodalite cages. [36]

The CO experiments were made using zeolites ZSM-5 and BEA. However, ZSM-5 is currently a work in progress at the Birchall Centre, so it will not be mentioned in this report. In zeolite BEA, at around 2200 cm^{-1} appears a peak, the CO area, when the CO is first injected. Then it reappears after the 2 injections (nonane + CO), which means that CO is interacting with LAS whether there is nonane in the molecule or not. The LAS are visible in the spectra, and they should only be about 50% after the CO injection. Since CO is not strong enough to displace nonane, it might mean that all the LAS are on the external surface, which is not very usual. So, conclusions cannot be drawn from this experiment alone (figure 43).

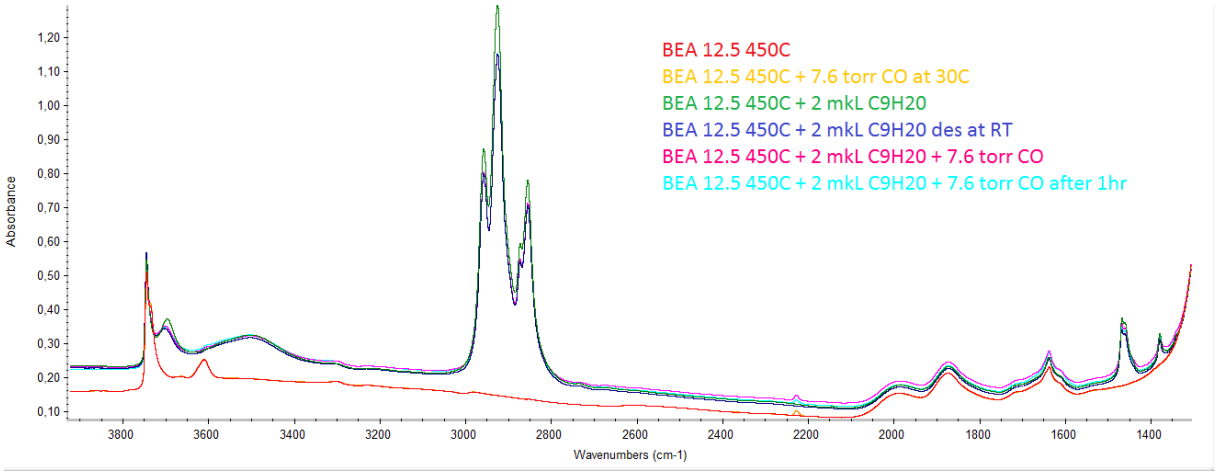

Figure 43 -IR spectra of the C9H20 + CO experience in zeolite BEA

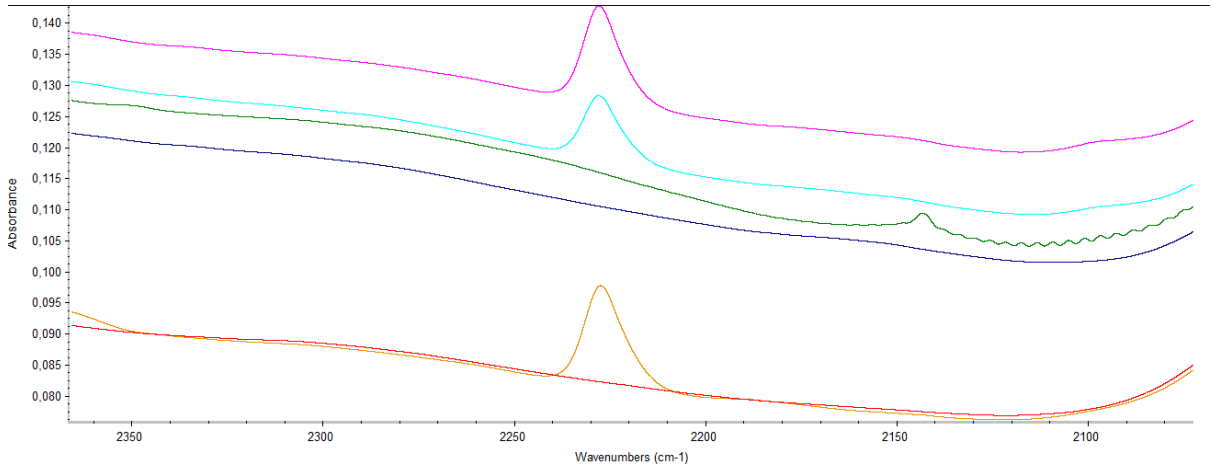

Figure 44 - IR spectra of the C9H20 + CO experience in zeolite BEA zoomed in the CO region

Around 2143 cm^{-1} a peak appears, which can be attributed to the CO gas phase (figure 44). In the OH region, it can be seen that the internal and external silanols disappeared completely, and the external are progressively releasing from nonane (figure 45). It is possible to distinguish between external and internal:

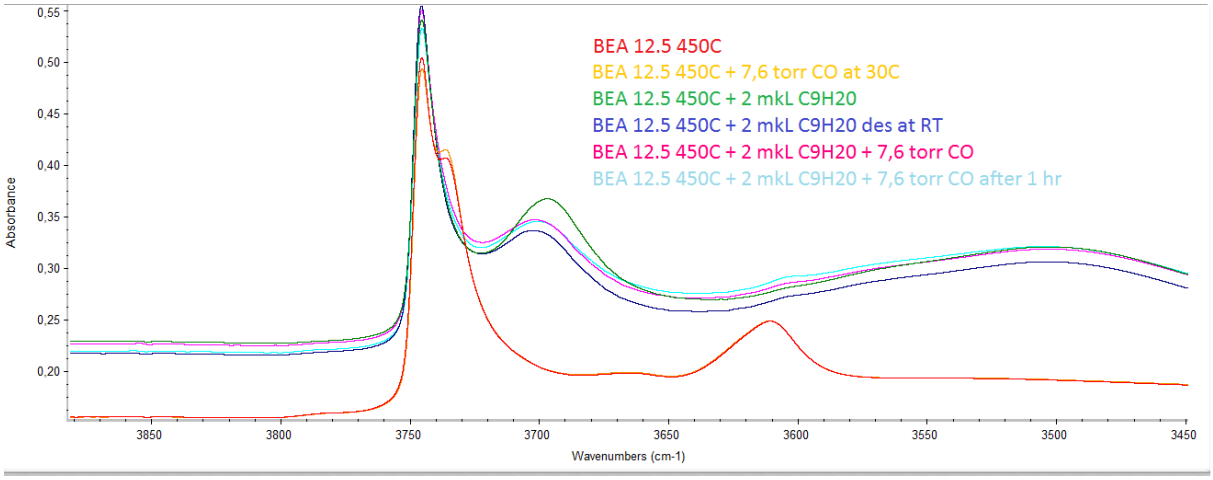

Figure 45 - IR spectra of the C9H20 + CO experience in zeolite BEA zoomed in the OH region

It should be noted that different zeolites have different pore size. In the zeolites in study, nonane occupies all the pore space, which means that if another molecule can penetrate the pores, it is displacing nonane. The following table summarizes the pore sizes of the 3 zeolites used in this work.

Table 12 - Pore size of zeolites Y, ZSM-5 (MFI) and BEA

Zeolite	Pore size
Y	≈7,5
MFI	≈5,5
BEA	≈5,6

The spectra of the pyridine desorptions showed that the samples prepared by route 2 have more Brønsted acid sites and the ones prepared by route 1 have more Lewis acid sites. The intensity of all OH groups (silanols and bridging OH groups in small and large cages) was higher in the samples prepared by route 2, an indication that route 2 is preferable. It was observed that low frequency (LF) OH groups were almost not accessible to pyridine, while high frequency (HF) OH groups and silanols were all accessible. Despite LF groups having very poor accessibility, they were more accessible in samples prepared by route 2. After the mesoporous treatment, the samples showed an increase in LAS and a decrease in BAS, comparing to sample 1 (NH4Y IE).

Accessibility experiments were also made in this work. A substituted pyridine (di-t-Bu-Py) was used, and was expected not to enter the zeolite's pores (7,5 Å), due to its big dimensions (7 Å). In fact, by comparing its spectra with the one from pyridine injection, it should be possible to distinguish between acid sites in the external and internal surface. However, di-t-Bu-Py was able to enter the zeolite Y's micropores. Tri-isopropylbenzene, whose kinetic diameter is 9,3 Å, is too big to enter the zeolite's pores. So, comparing its spectra with the one from pyridine, it showed the existence of some LAS in the external surface (in the form of EFAL species). The next molecule used was deuterated acetonitrile. As expected, since it is a small molecule (4 Å), it was able to access all OH groups, so it would be a good probe molecule to use. Nonane was also experimented and the result was as expected: it was able to interact with all OH groups. So, an experience combining the two probe molecules was made: nonane was injected first, and then CD_3CN. It was not successful though, because the CD_3CN was displacing the existing nonane and entering the pores. Hence, CO was used as the second probe molecule. However, it was firstly experimented in zeolites BEA and ZSM-5.

Zeolite BEA showed a peak from the CO, when it was injected first, and when it was injected after nonane, which means that CO is interacting with the LAS. This result was not expected, given that CO is not strong enough to displace nonane, and so it was theorized that maybe all the LAS were in the external surface. However, that is very unlikely.

5. Conclusions

The main goal of this work was to create mesopores in zeolite Y, for further use in biodiesel catalysis. This work was part of an ongoing investigation on the subject, which also involves other researchers, and was developed in the Birchall Centre at Keele University.

Since the optimum sequence of operations to do this was unknown, two routes were experimented. Route 1 consisted firstly in ion exchange to NH_4Y, and secondly undergoing a Surfactant Templated treatment. Route 2 was first treated with the Surfactant Templated method and then ion exchanged to ammonium form (figure 9). Besides the order of the operations, the optimum amount of citric acid used in the mesoporous treatment was also unknown for this zeolite. Thus, two different amounts of citric acid were used (6 meq and 4,5 meq). The samples were labelled as shown in table 4.

Besides the ion exchange and the mesoporous treatment, it was also experimented a calcination between the ion exchange and the mesoporous treatment, but it was disregarded because the sample lost almost all of its crystallinity.

Sorption experiments showed higher degree of mesoporosity in sample 5 (NaY 6), but since it had some crystallinity loss, it can be attributed to amorphous material. Nonetheless, route 2 was considered a better way of creating mesopores.

SEM/EDS analysis was run in all samples. The results showed an increase in the Si/Al in all treated samples. This was as expected, since the creation of mesopores causes dealumination.

The XRD results were used to calculate crystallinity and unit cell dimension (to calculate Si/Al ratio in the framework). Since there were some discrepancies in the crystallinity results, the same calculations were made to the samples with a silicon standard. Given that using an internal standard is more accurate and that those results were more consistent, it was chosen to consider the crystallinity percentages obtained with the internal standard. It was concluded that the optimum amount of citric acid

is 4,5 meq. Regarding the unit cell dimensions, as expected, the samples with more mesopores have the smaller unit cell size due to some dealumination by the citric acid.

FTIR was performed to quantify the acid sites in zeolite Y and to discriminate between acid sites in the external (mesopores) and internal (micropores) surface. To quantify the acid sites, pyridine adsorption was made, followed by desorption at different temperatures (150,200,250,300,350,400 and 450 ºC).

Several accessibility tests were made in this work. The accessibility of hydroxyls is connected to their location, as those in the external surface are usually accessible, while the accessibility of those in pores depends on the size of the guest molecule. Also, it should be noted that it depends on the experimental conditions. Naturally, the more mesoporous the sample is, the easier it is to access OH groups.

The overall results have shown that the Surfactant Templated Treatment was more successful using route 2, given that it showed small crystallinity loss and reasonable amount of mesopores. The mesoporous samples had a decrease on the amount of Brønsted sites and an increase of the Lewis sites, as expected.

It should be noted that the choice of characterization techniques and their operating parameters should always be taken into careful consideration. Often, spectroscopic techniques have certain limitations and results can be misleading, so the combination of different characterization techniques allows for a much more complete and accurate analysis of the properties of the samples.

.

6. Future Work

Future work should now be done to further test the accessibility, by running the same experiments on zeolite Y and comparing the results. Also, other probe molecules can be used, such as other substituted pyridines (lutidine and collidine), to characterize hydroxyls. Moreover, thermogravimetric analysis (TGA) could also be employed to determine the concentration of catalytic sites. Another two useful techniques that could be used to complete the characterizations made in this work are solid-state NMR spectroscopy, with special reference to ^{29}Si MAS NMR (magnetic-angle spinning) and solid-state ^{27}Al NMR. [46] Magnetic angle spinning is a technique used in NMR experiments that allows the determination of the $Si/Al_{framework}$, and ^{27}Al NMR can be used to verify the presence of EFAL species in a sample.

References

[1] - Cui, Q., Zhou, Y., Wei, Q., et al (2012). Role of the zeolite crystallite size on hydrocracking of vacuum gas oil over NiW/Y-ASA catalysts. In *Energy and Fuels* (Vol. 26, pp. 4664–4670).

[2] - Zhao, Y., Liu, Z., Li, W., et al (2013). Synthesis, characterization, and catalytic performance of high-silica y zeolites with different crystallite size. *Microporous and Mesoporous Materials*, *167*, 102–108.

[3] - Alan Dyer. (1988). *An Introduction to Zeolite Molecular Sieves*.

[4] - Derouane, E. G., Védrine, J. C., Ramos Pinto, R., et al (2013). The acidity of zeolites: Concepts, measurements and relation to catalysis: A review on experimental and theoretical methods for the study of zeolite acidity. *Catalysis Reviews - Science and Engineering*, *55*(4), 454–515.

[5] - Carrott, M. M. (2008). *Physisorption of gases by solids: Fundamentals, Theories and Methods for the Textural Characterization of Catalysts*. In *Catalysis: from Theory to Application*.

[6] - Cejka, J., Bekkum, H. van, Corma, A., & Schueth, F. (2007). *Introduction to Zeolite Science and Practise*. *Studies in Surface Science and Catalysis* (Vol. 168).

[7] - Xu, R., Pang, W., Yu, J., Huo, Q., & Chen, J. (2010). *Chemistry of Zeolites and Related Porous Materials: Synthesis and Structure*.

[8] - Basics of zeolites. (2016). In *Advanced Structured Materials* (Vol. 78, pp. 5–31).

[9] - Shi, J., Wang, Y., Yang, W., Tang, Y., & Xie, Z. (2015). Recent advances of pore system construction in zeolite-catalyzed chemical industry processes. *Chem. Soc. Rev.*, *44*(24), 8877–8903.

[10] - Guisnet, M., & Gilson, J.-P. (2014). CATALYTIC SCIENCE SERIES — VOL. 3. Retrieved from https://www.researchgate.net/profile/M_Guisnet/publication/230605057_Zeolites_for_Cleaner_Technologies/links/55ade3a108aee079921e3dc1/Zeolites-for-Cleaner-Technologies.pdf

[11] - Boronat, M., & Corma, A. (2015). Factors Controlling the Acidity of Zeolites. In *Catalysis Letters*, *145*(1), 162–172.

[12] - Shah, R., Payne, M., & Gale, J. (1997). Acid-base catalysis in zeolites from first principles. In *International Journal of Quantum Chemistry*, *61*, 393–398.

[13] - Bordiga, S., Lamberti, C., Bonino, F., Travert, A., & Thibault-Starzyk, F. (2015). Probing zeolites by vibrational spectroscopies. *Chem. Soc. Rev.*, *44*(20), 7262–7341.

[14] - Coster, D., Blumenfeld, A. L., & Fripiat, J. J. (1994). Lewis Acid Sites and Surface Aluminum in Aluminas and Zeolites: A High-Resolution NMR Study. In *The Journal of Physical Chemistry*, *98*(24), 6201–6211.

[15] - Vimont, A., Thibault-Starzyk, F., & Daturi, M. (2010). Analysing and understanding the active site by IR spectroscopy. In *Chemical Society Reviews*, *39*(12), 4928.

[16] - James J Spivey. (2007) Catalysis. In Royal Society of Chemistry, volume 16

[17] - Weitkamp, J. (2000). Zeolites and catalysis. In *Solid State Ionics*, *131*(1), 175–188.

[18] - Xu, B., Bordiga, S., Prins, R., & van Bokhoven, J. A. (2007). Effect of framework Si/Al ratio and extra-framework aluminum on the catalytic activity of Y zeolite. In *Applied Catalysis A: General*, *333*(2), 245–253.

[19] - García-Martínez, J., Johnson, M., Valla, J., Li, K., & Ying, J. Y. (2012). Mesostructured zeolite Y—high hydrothermal stability and superior FCC catalytic performance. In *Catalysis Science & Technology*, *2*(5), 987.

[20] - Li, K., Valla, J., & Garcia-Martinez, J. (2014). Realizing the commercial potential of hierarchical zeolites: New opportunities in catalytic cracking. In *ChemCatChem*.

[21] - Ertl, G., Knözinger, H., & Weitkamp, J. (2008). *Ion exchange and impregnation*. *Handbook of Heterogeneous Catalysis* (Vol. 105350616). DOW Chemical Company Elsevier.

[22] - Sultan, E.A., Selim, M. M. (1989). Effect of dealumination of NH4Y-zeolite on the Cristallinity, Thermal Stability and Catalytic Activity in Cumene Cracking.pdf. In *Catalytic Activity in Cumene Cracking*.

[23] - Avhad, M. R., & Marchetti, J. M. (2016). Innovation in solid heterogeneous catalysis for the generation of economically viable and ecofriendly biodiesel: A review. *Catalysis Reviews - Science and Engineering*, *58*(2), 157–208.

[24] - Che, M., & Védrine, J. (2012). Surface Area/Porosity, Adsorption, Diffusion. In *Characterization of solid materials and heterogeneous catalysts*, Vol. 2(pp. 853–881).

[25] - Thommes, M., Kaneko, K., Neimark, A. V., et al (2015). Physisorption of gases, with special reference to the evaluation of surface area and pore size distribution (IUPAC Technical Report). In *Pure and Applied Chemistry*, *87*(9–10), 1051–1069.

[26] - Chester, A. W., & Derouane, E. G. (2010). Powder Diffraction in Zeolite Science: An Introductory Guide. In *Zeolite characterization and catalysis: A tutorial* (pp. 1-64).

[27] - https://www.slideshare.net/meonly21Icandependonhimallmylife AA/xrd-lecture-1

[28] - Fultz, B., & Howe, J. (2013). Diffraction and the X-Ray Powder Diffractometer. In *Transmission Electron Microscopy and Diffractometry of Materials SE - 1* (pp. 1–57).

[29] - Australian Microscopy & Microanalysis Research Facility: My scope, [Online] Available: http://li155-94.members.linode.com/myscope/xrd/background/machine/

[30] - Materials Research Laboratory at UCSB: X-ray basics, [Online] Available: https://www.mrl.ucsb.edu/centralfacilities/x-ray/basics

[31] - ASTM D3942-03(2013). (2015). *Standard Test Method for Determination of the Unit Cell Dimension of a Faujasite-*. *Standard Test Method for Determination of the Unit Cell Dimension of a Faujasite-Type Zeolite* (Vol. 53)

[32] - Chester, A. W., & Derouane, E. G. (2010). Infrared and Raman Spectroscopy. In *Zeolite characterization and catalysis: A tutorial* (pp. 197-222).

[33] - Chemistry LibreTexts: How an FTIR Spectrometer Operates, [Online] Available: https://chem.libretexts.org/Core/Physical_and_Theoretical_Chemistry/Spectroscopy/Vibrational_Spectroscopy/Infrared_Spectroscopy/How_an_FTIR_Spectrometer_Operates

[34] - Che, M., & Védrine, J. (2012). Infrared Spectroscopy. In *Characterization of solid materials and heterogeneous catalysts,* Vol 1, (pp. 3–45).

[35] - Smith, B. (2011). *Fundamentals of Fourier transform infrared spectroscopy*. *Vasa* (Vol. 40).

[36] - Hadjiivanov, K. (2014). Identification and Characterization of Surface Hydroxyl Groups by Infrared Spectroscopy. In *Advances in Catalysis*.

[37] - Goldstein, J. I., Newbury, D. E., Lyman, C. E., & Joy, D. C. (1992). Scanning Electron Microscopy and X-Ray Microanalysis. In *Handbook of Analytical Methods for Materials* (pp. 21–363).

[38] - Chester, A. W., & Derouane, E. G. (2010). Electron Microscopy and Imaging. In *Zeolite characterization and catalysis: A tutorial* (pp. 169-196).

[39] - ASTM. (2012). *Standard Test Method for Determination of Relative X-ray Diffraction Intensities of Faujasite-Type Zeolite-Containing Materials*, *i*(Reapproved 2008), 1–7.

[40] - Guisnet, M., & Ribeiro, F. R. (2006). *Les zeolithes - un nanomonde au service de la catalyse*.

[41] - Loughlin, K. F., Al-Khattaf, S. S., & Zaman, S. F. (2005). *Kinetics of Sorption of 1,3 Di-Isopropyl Benzene and 1,3,5 Tri-Isopropyl Benzene in Nay Crystals, Alumina Matrix and FCC Catalyst Particles by Zero Length Column Method*, (1–20), Retrieved from http://folk.ntnu.no/skoge/prost/proceedings/aiche-2005/non-topical/Non topical/papers/120c.pdf

[42] - Pelmenschikov, A. G., Van Santen, R. A., Jãnchen, J., & Meijer, E. (1993). CD3CN as a probe of Lewis and Bronsted acidity of zeolites. In *Journal of Physical Chemistry*, *97*(42), 11071–11074.

[43] - Soltanov, R. I., Paukshtis, E. A., & Yurchenko, E. N. (1887). Application of deuteroacetonitrile to characterize surface aprotic acidic centers on heterogeneous catalysts. In *Reaction Kinetics, Mechanisms adn Catalysis* (Vol. 34, pp. 421–426).

[44] - Grillet, Y., Llewellyn, P. L., Kenny, M. B., Rouquerol, F., & Rouquerol, J. (1993). Evaluation of the n-nonane preadsorption method with a well characterized model adsorbent: Silicalite-I. *Pure and Applied Chemistry*, *65*(10), 2157–2167.

[45] - Forghani, A. A., Lewis, D. M., & Pendleton, P. (2017). Catalytic Hydro-Cracking of Bio-Oil to Bio-Fuel. In *Biodegradation and Bioconversion of Hydrocarbons* (pp. 205–223).

[46] - Chester, A. W., & Derouane, E. G. (2010). Solid-State NMR Spectroscopy. In *Zeolite characterization and catalysis: A tutorial* (pp. 65-105).

APPENDIX

APPENDIX A – Sorption Experiments

Table A1 - MultiPoint BET and t-plot method (external and micropore) surface area for all samples

	Sample	MultiPoint BET area (m2/g)	t-method external area (m2/g)	t-method micropore area (m2/g)
NH4Y	1	286,1	126,1	160
NH4Y 6	2	714,9	191	523,9
NH4Y 6 calcined	3	490,5	490,5	-
NH4Y 4.5	4	632,4	479,6	152,8
NaY 6	5	634,6	506,8	127,8
NaY 4.5	6	455,3	233,6	221,8
original NaY		210,2	87,3	122,9
original NH4Y		423,2	156,3	266,9

Table 13 - t-plot method micropore volume and DFT pore diameter for all samples

	Sample	t method micropore volume (cm3/g)	DFT micropore diameter (Å)	DFT mesopore diameter (Å)
NH4Y	1	0,07	8,63	
NH4Y 6	2	0,25	11,14	
NH4Y 6 calcined	3	-	37,76	37,75
NH4Y 4.5	4	0,07	11,14	37,75
NaY 6	5	0,06	9,82	42,52
NaY 4.5	6	0,14	11,14	31,79
original NaY		0,08	8,63	
original NH4Y		0,18	9,82	

APPENDIX B – XRD patterns for all samples

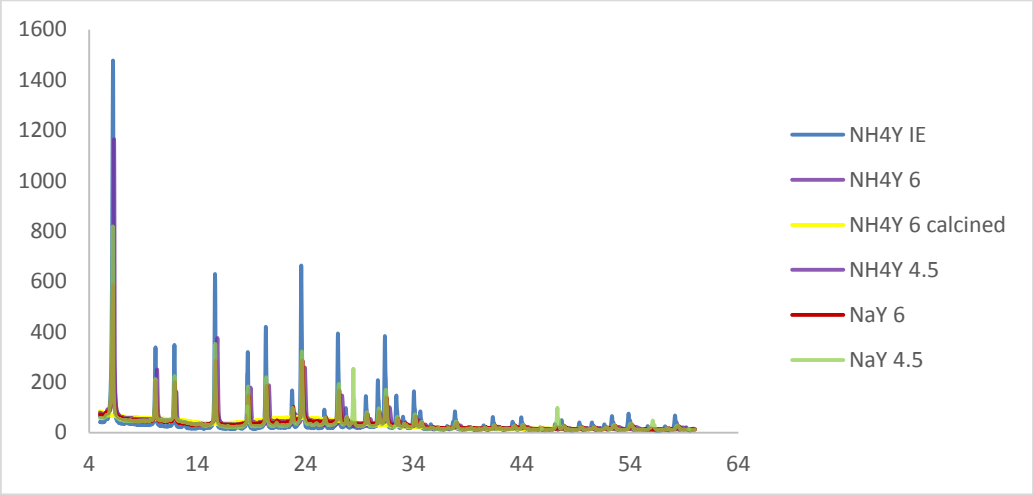

APPENDIX C – SEM/EDS spectra for all samples

Figure 46 – NH4Y IE

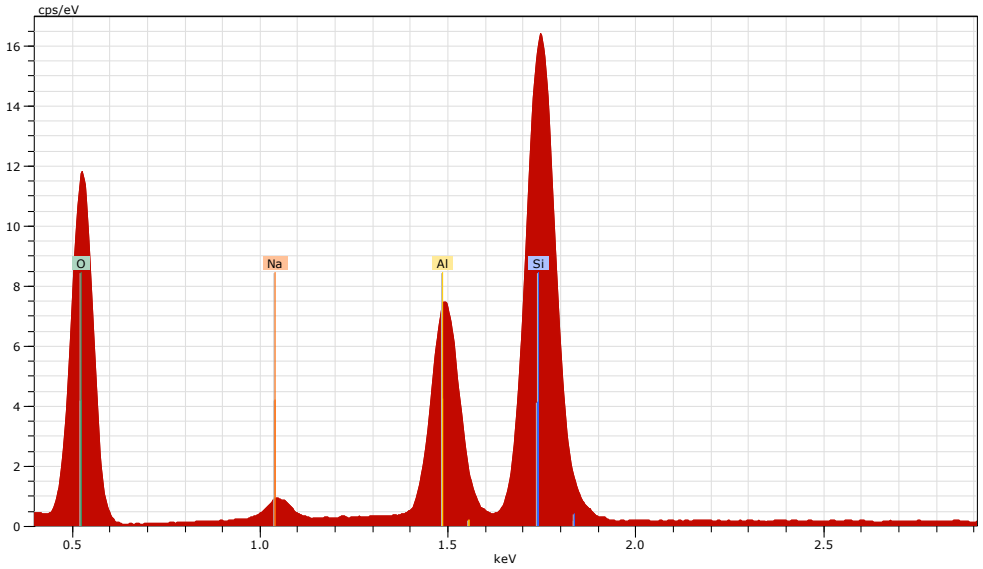

Figure 47 – NH4Y 6

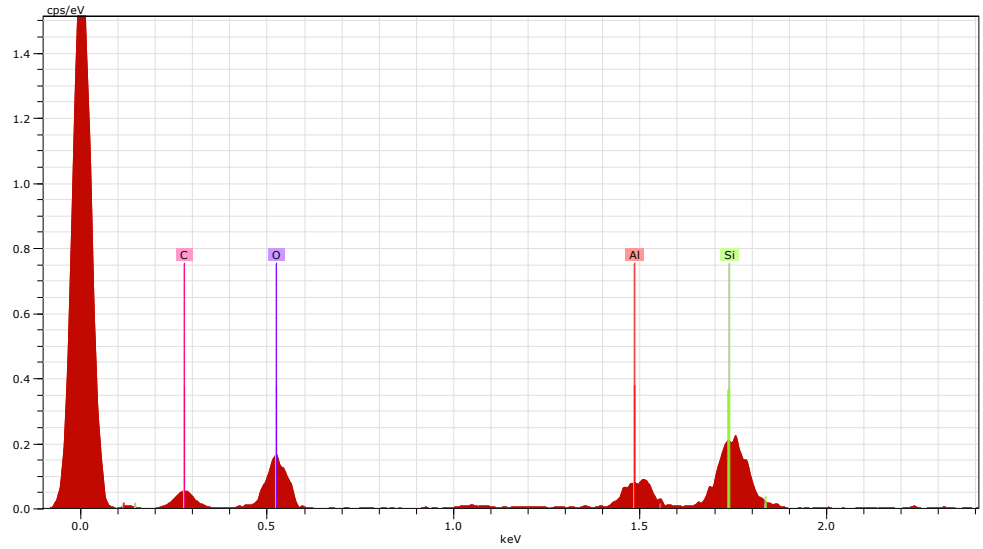

Figure 48 - NH4Y 6 calcined

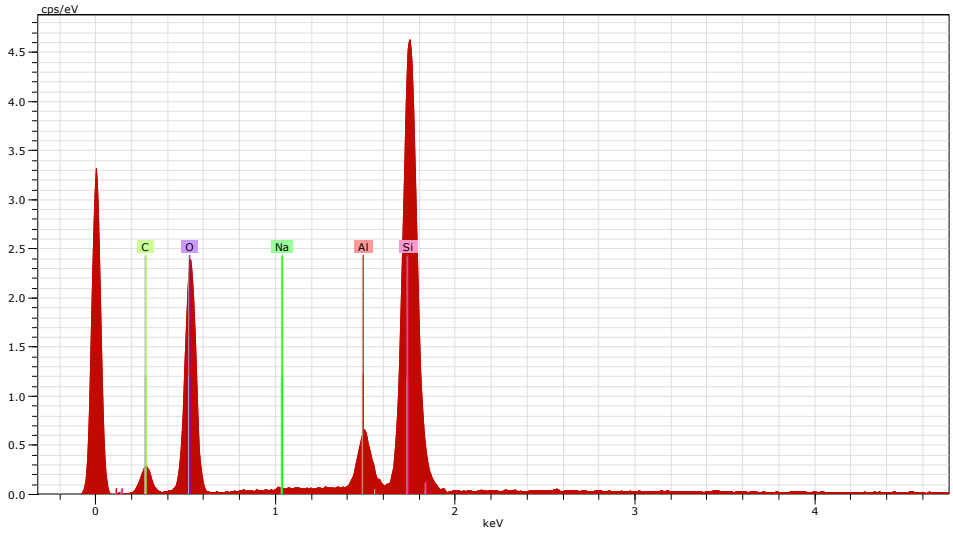

Figure 49 - NH4Y 4.5

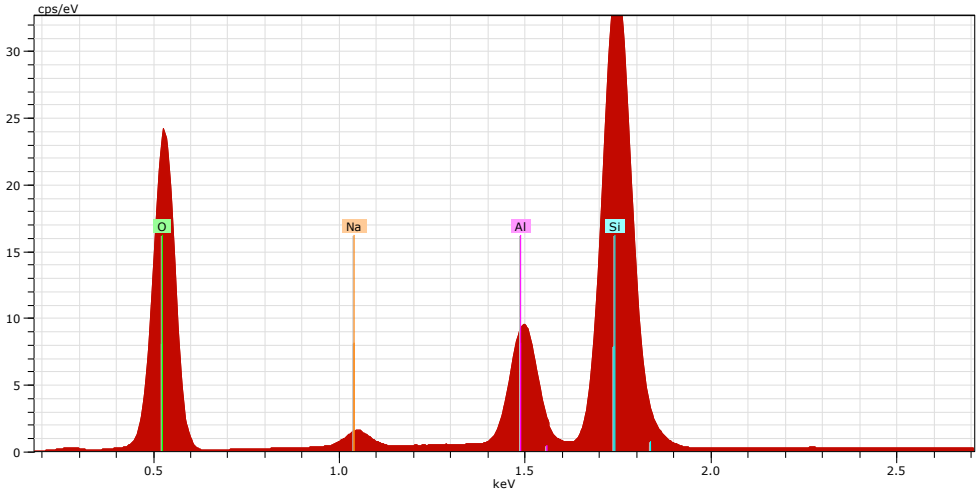

Figure 50 – NaY 6

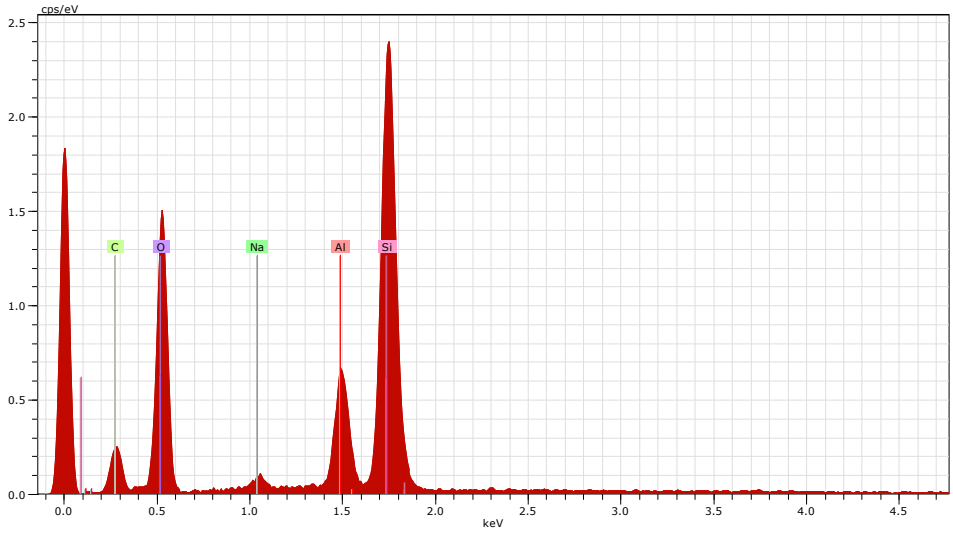

Figure 51 - NaY 4.5

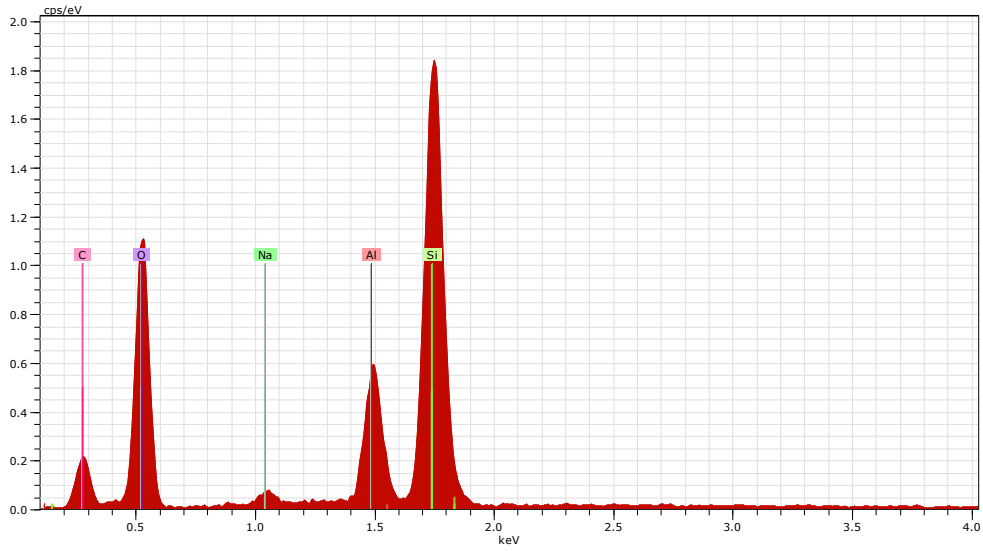

APPENDIX D – IR

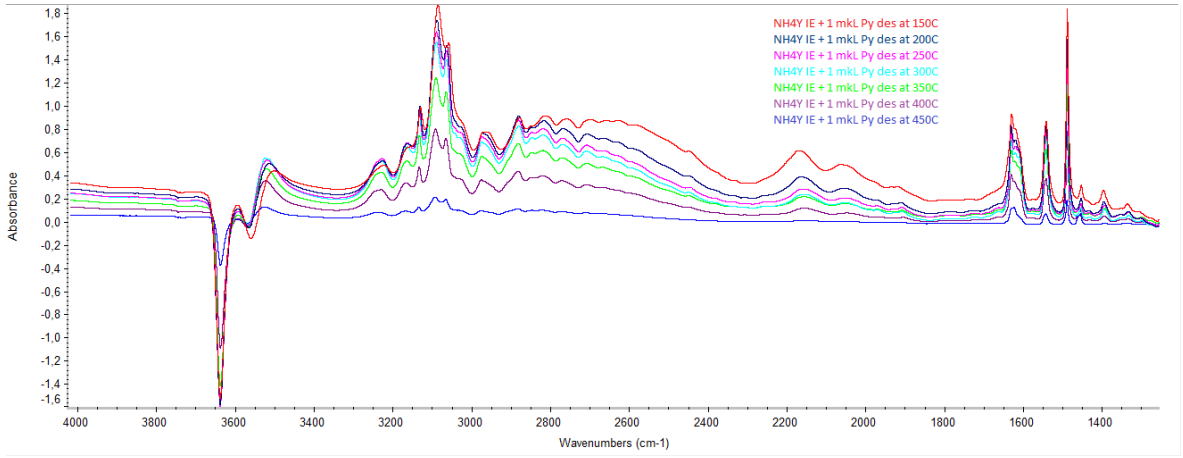

Figure 52 – IR spectra of pyridine desorption at different temperatures subtracted by spectra before pyridine injection for sample 1

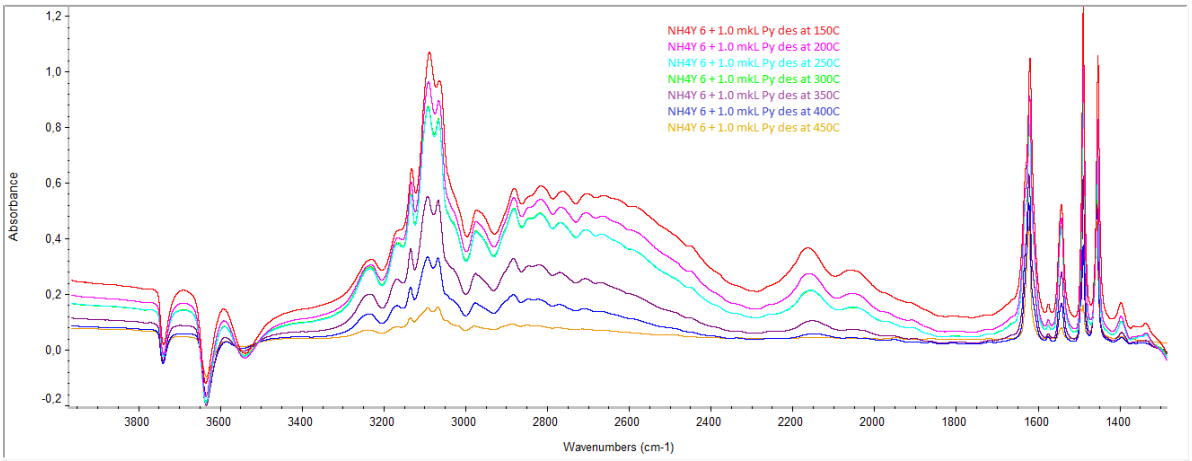

Figure 53 - IR spectra of pyridine desorption at different temperatures subtracted by spectra before pyridine injection for sample 2

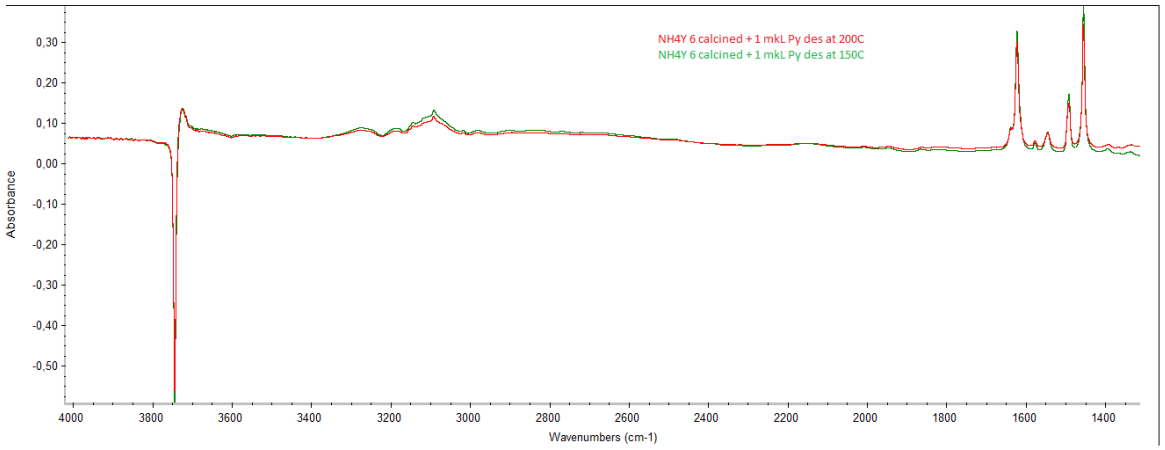

Figure 54 - IR spectra of pyridine desorption at different temperatures subtracted by spectra before pyridine injection for sample

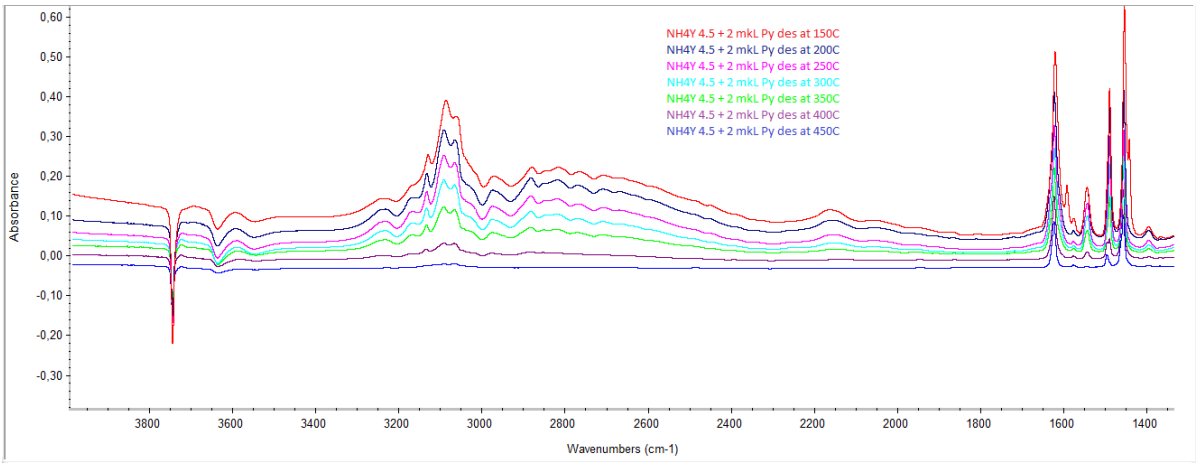

Figure 55 - IR spectra of pyridine desorption at different temperatures subtracted by spectra before pyridine injection for sample 4

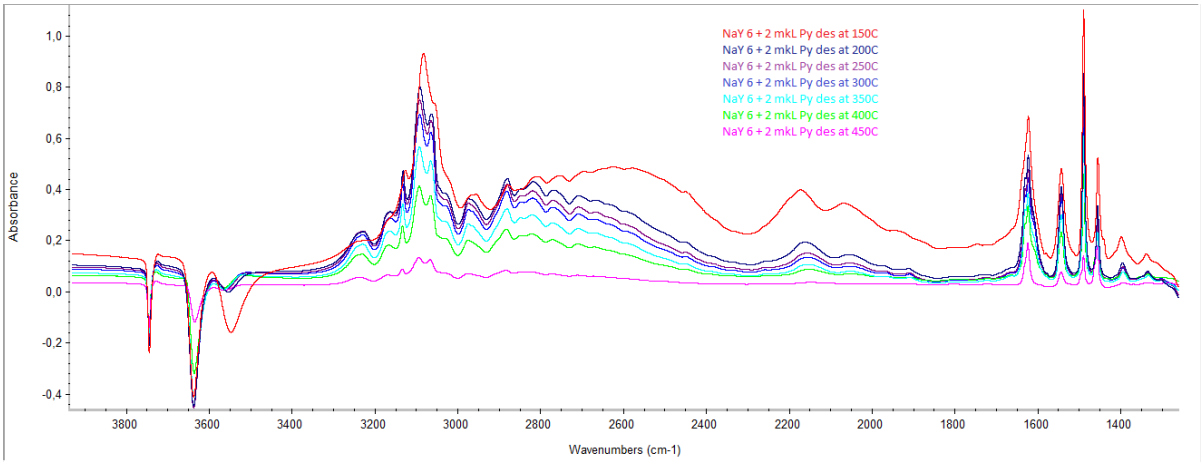

Figure 56 - IR spectra of pyridine desorption at different temperatures subtracted by spectra before pyridine injection for sample 5

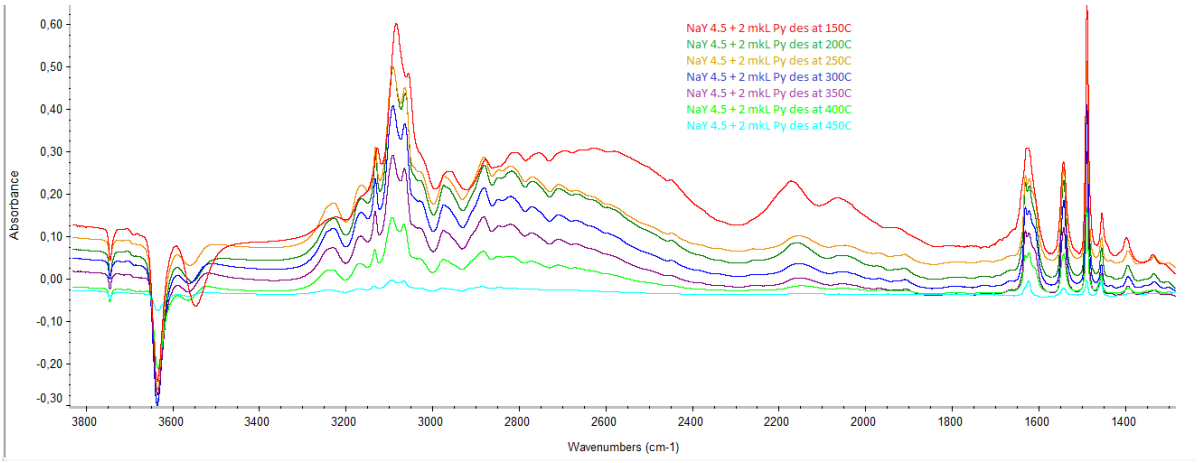

Figure D6 – IR spectra of pyridine desorption at different temperatures subtracted by spectra before pyridine injection for sample 6

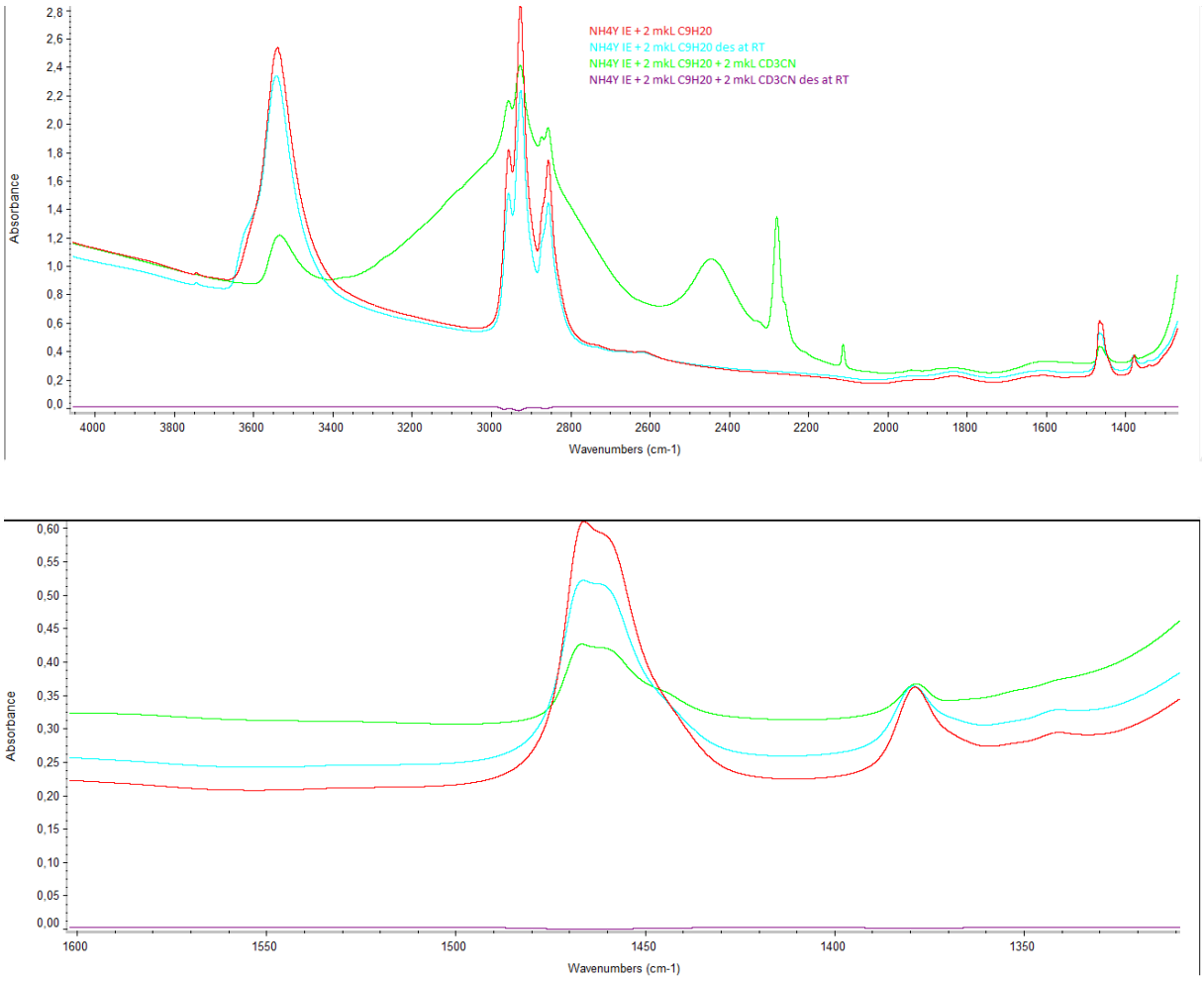

Figure 57 - IR spectra C9H20 adsorption followed by CD3CN adsorption for sample 1, and zoom in the BAS and LAS zone